Siberian Traps volcaniclastic rocks and the role of magma-water interactions

Benjamin A. Black[1,†], Benjamin P. Weiss[2,†], Linda T. Elkins-Tanton[3,†], Roman V. Veselovskiy[4,5,†], and Anton Latyshev[4,5,†]

[1]*Department of Earth and Planetary Science, University of California, Berkeley, California 94720, USA*
[2]*Department of Earth, Atmospheric, and Planetary Sciences, Massachusetts Institute of Technology, Cambridge, Massachusetts 02139, USA*
[3]*School of Earth and Space Exploration, Arizona State University, Tempe, Arizona 85287, USA*
[4]*Schmidt Institute of Physics of the Earth, Russian Academy of Sciences, 123995 Moscow, Russia*
[5]*Faculty of Geology, Lomonosov Moscow State University, 119991 Moscow, Russia*

ABSTRACT

The Siberian Traps are one of the largest known continental flood basalt provinces and may be causally related to the end-Permian mass extinction. In some areas, a large fraction of the Siberian Traps volcanic sequence consists of mafic volcaniclastic rocks. Here, we synthesize paleomagnetic, petrographic, and field data to assess the likely origins of these volcaniclastic rocks and their significance for the overall environmental impact of the eruptions. We argue that magma-water interactions, including both lava-water interactions and phreatomagmatic explosions in vents, were important components of Siberian Traps magmatism. Phreatomagmatic episodes may have generated tall water-rich eruption columns, simultaneously promoting removal of highly soluble volcanic gases such as HCl and potentially delivering additional sulfur to the upper atmosphere.

INTRODUCTION

Volcaniclastic rocks within the Siberian Traps large igneous province (Ross et al., 2005) are widely recognized but poorly understood and documented. Detailed accounts of these volcaniclastic rocks vary considerably. The thickness of volcaniclastic material ranges from intercalated layers less than a meter thick on the Putorana Plateau (Büchl and Gier, 2003) to hundreds of meters near the base of the volcanic sections in Angara (Naumov and Ankudimova, 1995) and in the Maymecha-Kotuy area (Fedorenko et al., 2000; Fedorenko and Czamanske, 1997). The total volume of mafic volcaniclastic material has been estimated at >200,000 km^3 (Ross et al., 2005), or >5% of the total volume of the Siberian Traps (Malich et al., 1974; Reichow et al., 2009).

The eruption of the Siberian Traps overlaps within geochronologic uncertainty with the catastrophic end-Permian mass extinction (Kamo et al., 2003; Reichow et al., 2009; Burgess et al., 2014). Consequently, Siberian Traps magmatism has been widely invoked as a direct or indirect trigger for the extinction, which began at 251.941 ± 0.037 Ma and lasted 60 ± 48 k.y. (Burgess et al., 2014). However, the precise causal mechanisms linking magmatism to extinction remain poorly understood. Carbon release from the Siberian Traps has been cited to explain global warming across the Permian-Triassic boundary (Joachimski et al., 2012; Sun et al., 2012); the climate effects of volcanic CO_2 do not depend on injection altitude (Williams et al., 1992; Wignall, 2001). While the enormous volume and rich volatile budget of the Siberian Traps could also produce large fluxes of sulfur and halogen gases (Black et al., 2012, 2014a), explosive delivery of those gases to the stratosphere is a prerequisite for lasting global environmental effects (e.g., White, 2002; Wignall, 2001; Black et al., 2012).

Recent work suggests that flood basalt volcanism may span the spectrum from effusive to explosive. During episodes of particularly high mass flux, fire fountaining may result in eruption columns tall enough to breach the high-latitude tropopause (Glaze et al., 2015). Proximal scoria falls, clastogenic lava flows, and welded spatter near the Roza vent system of the 16 Ma Columbia River flood basalts in Washington denote episodes of pyroclastic activity (Brown et al., 2014; Self et al., 1997; Thordarson and Self, 1998). Similarly, the historic Laki fissure eruption in Iceland was characterized by episodic explosive pulses accompanied by ash fall and often followed by a pulse of lava emplacement (Thordarson et al., 2003; Thordarson and Self, 1993). In a further example that may be particularly relevant to the genesis of Siberian Traps mafic volcaniclastic rocks, similar rocks in the Transantarctic Mountains associated with the Jurassic Ferrar large igneous province have been interpreted as the products of an extraordinarily large phreatomagmatic vent complex in the Coombs Hills (McClintock and White, 2006; White and McClintock, 2001; Ross and White, 2006). Volcaniclastic rocks from some Siberian localities distinctly resemble descriptions from the Coombs Hills and may represent periods of similar phreatomagmatic activity during the early phases of eruption of the Siberian Traps.

The extent and style of explosive volcanism during the emplacement of the Siberian Traps could have far-reaching consequences. If a large fraction of the mafic volcaniclastic rocks were originally fragmented through explosive processes, they could represent one of the largest mafic pyroclastic assemblages known in the rock record. Perhaps more importantly, the type and intensity of explosive activity influence plume heights and the fate of volcanic gases.

The nomenclature of fragmented volcanic rocks is complex and occasionally contradictory. Throughout this article, we follow the nomenclature of White and Houghton (2006). Among volcaniclastic rocks the terms tuff, lapilli tuff, tuff breccia, and breccia refer to grain size in ascending order, from ash to lapilli to blocks and bombs. Volcaniclastic rocks are lithified

†E-mails: bblack@berkeley.edu, bpweiss@mit.edu, ltelkins@asu.edu, roman.veselovskiy@ya.ru, anton.latyshev@gmail.com.

GSA Bulletin; September/October 2015; v. 127; no. 9/10; p. 1437–1452; doi: 10.1130/B31108.1; 8 figures; 2 tables; Data Repository item 2015161; published online 30 April 2015.

deposits of fragments produced and/or transported during the course of a volcanic eruption, including everything from fallout to pyroclastic density current deposits to fluvially transported syneruptive volcanic materials (White and Houghton, 2006). In contrast, epiclastic deposits include the transported weathering products of volcanic rocks that have been reshaped and resized relative to the original volcanic fragments (White and Houghton, 2006).

Emplacement temperatures should differ depending on the origins of volcaniclastic rocks. Epiclastic rocks should be emplaced at ambient surface temperatures. Lahars can emplace warmer material, but temperatures will nonetheless be less than 100 °C (e.g., Pierson et al., 1996). In contrast, the emplacement temperatures of pyroclastic rocks can reach near-magmatic temperatures. Emplacement temperatures of pyroclastic density currents with little external water should significantly exceed 100 °C, ranging up to >580 °C (e.g., McClelland and Druitt, 1989; McClelland et al., 2004; Paterson et al., 2010). The emplacement temperatures of phreatomagmatic pyroclastic density currents are expected to be slightly cooler due to incorporation of external water (Koyaguchi and Woods, 1996; McClelland et al., 2004) and span a range from ~100 °C to >300 °C (Cioni et al., 2004; Porreca et al., 2008).

In this paper, we classify the Siberian Traps volcaniclastic rocks into six preliminary lithofacies. Among these lithofacies, the massive rocks are the most difficult to interpret on the basis of textural features alone. We apply paleomagnetic measurements to help distinguish pyroclastic rocks emplaced at high temperatures from other fragmental rocks. We find paleomagnetic and volcanological evidence for a range of magma-water interactions and occasional pyroclastic episodes. The extent to which such eruptions increased global environmental stresses depends on the frequency with which eruption columns reached the stratosphere.

METHODS AND GEOLOGIC BACKGROUND

Field work is challenging in north-central Siberia. Siberian Traps sections are exposed primarily along river valleys, making interregional correlations difficult. Our sample names reflect the locality of the sample, followed by the year of collection, followed by the section and sample number. For example, sample K08–11.6 was collected in 2008 on the Kotuy River, from section number 11. As shown in Figure 1A, we visited volcaniclastic sections on the Kotuy (K), Maymecha (M), Angara (A), and Nizhnyaya Tunguska (NT) rivers, as well as at Noril'sk (N), in the summers of 2006, 2008, 2009, 2010, and 2012. Table 1 contains a summary of our lithofacies classifications and interpretations, and Table 2 contains descriptions of all samples discussed in this paper. To allow labeling of individual samples in Figure 2, we have created alphabetical sample signifiers that are also

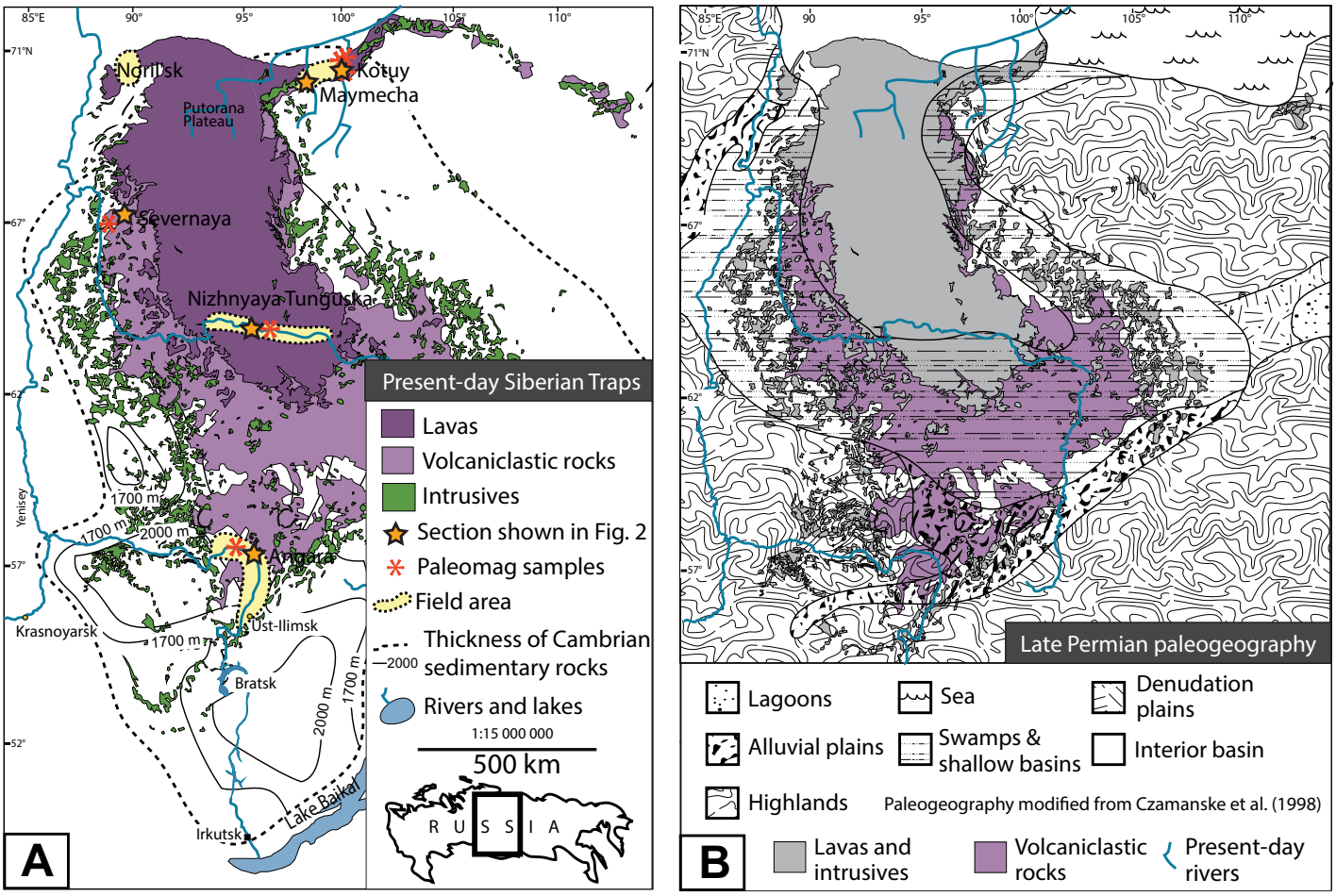

Figure 1. Map of the Siberian Traps showing our field areas and sampling locations, modified from Svensen et al. (2009) and Malich et al. (1974). (A) Present-day outcrop extent of lavas, volcaniclastic rocks, and intrusive rocks, with Cambrian carbonate and evaporite thicknesses from Zharkov (1984), (B) overlain with Late Permian paleogeography simplified from Czamanske et al. (1998).

TABLE 1. PRELIMINARY LITHOFACIES CLASSIFICATION OF SIBERIAN TRAPS VOLCANICLASTIC ROCKS AT LOCALITIES DENOTED ON FIGURE 1

Lithofacies	Description	Distribution	Interpretation
mj: massive tuff, lapilli tuff, or tuff breccia with primarily juvenile clasts	Massive, poorly sorted with fine- to medium-grained ash matrix. Abundant angular to rounded basaltic clasts (5–50 cm in diameter).	Kotuy River (~50%), Maymecha River (~45%), Angara River (~25%), Nizhnyaya Tunguska River	Difficult to determine from field observations alone. Rocks may originate from hyaloclastic, autoclastic, magmatic, or pyroclastic (phreatomagmatic or magmatic) processes (likely from some combination of all of these).
ml: massive tuff, lapilli tuff, or tuff breccia with abundant lithic clasts	Massive, poorly sorted with fine- to medium-grained ash matrix. Abundant sedimentary clasts ranging from angular to rounded.	Kotuy River (~30%), Angara River (~35%), Maymecha River (~10%). Inside diatremes (Svensen et al., 2009)?	Difficult to determine from field observations alone, but most consistent with phreatomagmatic pyroclastic density currents.
bLT: bedded tuff and lapilli tuff	Thinly to thickly bedded rocks (lapilli tuff is most common), typically lacking well-developed grain size sorting. Angular lapilli-sized juvenile and minor accidental clasts within a medium ash to lapilli-sized matrix.	Maymecha River (~30%), Angara River (~30%), Kotuy River (<5%), Nizhnyaya Tunguska River, Noril'sk	Originated in subaqueous hyaloclastic density currents and phreatomagmatic pyroclastic density currents.
bLTal: bedded tuff and lapilli tuff with accretionary lapilli	Thinly to thickly bedded fine tuff to lapilli tuff, often displaying well-sorted grains with normal grading, with accretionary lapilli.	Angara River (<10%), Kotuy River (<15%), Nizhnyaya Tunguska River, Noril'sk	Originated in pyroclastic density currents or fallout associated with phreatomagmatic eruption.
eLT: eutaxitic tuff and lapilli tuff	Welded and compacted tuff to lapilli tuff.	Maymecha River (<15%)	Produced by pyroclastic density currents.
dl: volcaniclastic dikes with abundant lithic clasts	Dikes with ash- to lapilli-sized basaltic and sedimentary fragments, typically 30 cm to 1 m in thickness.	Angara River (<1%), Ust-Ilimsk	Originated from interactions between magmas and wet sedimentary material.

Note: In the column listing distributions of each lithofacies, the values in parentheses denote the estimated volume percentage relative to the total volcaniclastic volume within each study area, where sufficient observations existed to warrant such an estimate.

listed in Table 2 along with cross-references to the full sample name. As described herein, we applied petrographic, volcanological, and paleomagnetic methods to investigate the volcaniclastic rocks.

Figure 2 compiles several composite stratigraphic sections showing occurrences and characteristics of Siberian volcaniclastic rocks as well as the stratigraphic positions of the samples we describe in this paper. The volcaniclastic rocks attain maximum reported thicknesses near the center of the Tunguska Basin; drill core suggests that mafic volcaniclastic units could reach 700 m in thickness at the base of the volcanic sequence near the Nizhnyaya Tunguska River (Levitan and Zastoina, 1985; Sharma, 1997; Zolotukhin and Almukhamedov, 1988). While the volcaniclastic rocks are particularly common in the lowest several hundred meters of the volcanic stratigraphy in many localities, the relatively well-studied Noril'sk section hosts intercalated basalts and tuffs, lapilli tuffs, and tuff breccias (Rudakova and Krivolutskaya, 2009). On the Maymecha River, the basal Pravoboyarsky Suite, which is dominantly composed of volcaniclastic units, reaches ~300 m in thickness (Fedorenko and Czamanske, 1997), while the corresponding Arydzhangsky Suite on the Kotuy River contains a smaller but still significant proportion of volcaniclastic units (Fedorenko et al., 2000). More detailed physical volcanological study of the large igneous province as a whole is urgently needed to assemble a complete portrait of the magmatic system and a chronology of the eruption.

Recent paleomagnetic studies of the Siberian Traps have focused on characterizing the magnetostratigraphy (Gurevitch et al., 2004; Pavlov et al., 2011; Veselovskiy et al., 2012), the implications of secular variation of the magnetic field for eruption time scales (Pavlov et al., 2011), and geomagnetic field paleointensities and the paleolatitude of Siberia (Veselovsky et al., 2003; Heunemann et al., 2004; Pavlov et al., 2007). Here, we use paleomagnetic studies to constrain emplacement temperatures of volcaniclastic rocks using techniques pioneered by Aramaki and Akimoto (1957) and Hoblitt and Kellogg (1979) as refined by Kent et al. (1981). The component of natural remanent magnetization (NRM) carried by ferromagnetic grains in lithic and cooled juvenile clasts with blocking temperatures above the emplacement temperature will be magnetized in random directions when comparing individual clasts. Grains with blocking temperatures below the emplacement temperature will be unidirectionally magnetized across multiple clasts. Consequently, for magnetite-bearing clasts emplaced at temperatures lower than the Curie temperature of

TABLE 2. SUMMARY OF FIELD, PETROGRAPHIC, AND PALEOMAGNETIC DATA FOR SELECTED VOLCANICLASTIC SAMPLES FROM THE SIBERIAN TRAPS

Region	Sample signifier	Full sample ID	GPS coordinates	Description	Componentry	Glass fragments	Paleomagnetic results
Angara	A	A10-A9B A10-7.1	102.370°E 58.878°N	Fig. 3A. Poorly sorted clasts include large stromatolitic limestone blocks and small rounded pebbles; rare lenses of well-sorted fine-grained tuff. Outcrop 50 m high. (ml)			N/A
	B	A10-3.5	102.122°E 58.940°N	Poorly sorted lithic-rich lapilli tuff with angular igneous clasts. (ml)	Feldspars: 25% plagioclase, 75% alkali feldspar, 50% albite.	Weakly to moderately vesicular with scalloped edges and mosaic cracks.	N/A
	C	A10-13.3	102.723°E 58.738°N	Abundant accretionary lapilli organized into low-angle cross-stratified and plane-parallel bed forms. Near base of cliff of volcaniclastic material ~200 m high. (bLTal)	60% juvenile, 40% accidental. Feldspars: 27% plagioclase, 73% alkali feldspar.	Equant unvesiculated altered, formerly glassy material fragments.	N/A
	D	A10-10.2	102.620°E 58.773°N	Volcaniclastic dike crosscutting lapilli tuff. Outcrop 10 m high. (dl)			N/A
Kotuy	E	K08-11.6	102.616°E 71.203°N	1-m-thick reddish accretionary lapilli–bearing lapilli tuff, intercalated with alkaline lavas, ~220 m above base of Arydzhangsky Suite. (bLTal)	90% juvenile, 10% accidental.	See Figure 4F. Poorly vesicular, equant altered, formerly glassy material fragments.	Uniformly magnetized at all temperatures (T).
	G	K08-7.11	102.590°E 71.181°N	Mafic lapilli tuff from near base of Arydzhangsky suite, sampled from float, 1–2 cm basaltic clasts within fine matrix. (bLT)	100% juvenile.		Uniformly magnetized at low T. Nonuniformly magnetized at high T. Emplacement at T = 270–340 °C?
	H	K08-7.10	102.590°E 71.181°N	Arydzhangsky Suite. (mj)	100% juvenile.		N/A
	I	K08-3.4	102.355°E 71.049°N	Arydzhangsky Suite. (mj)		Weakly to moderately vesicular with scalloped edges.	N/A
	J	K09-7.7	102.663°E 71.131°N	Pravoboyarsky Suite. Cliffy basal lapilli tuff capped by fine tuff with well-sorted plane-parallel beds 1–3 cm thick. ~8 m total thickness. (bLTal)			N/A
	K	K08-10.3	102.633°E 71.203°N	Steeply dipping 10–1- m-thick unit. Lahar or debris flow? (mj)			Randomly magnetized at all T. Cold emplacement?
	L	K09-10.4A	103.105°E 72.497°N	Pravoboyarsky Suite. Cliff-forming 30-m-thick tuff breccia, unconformable contact with underlying Tungusskaya sedimentary rocks, abundant unsorted 1–50 cm clasts of country rock including coal, limestone, and rounded pebbles. (ml)			N/A
Maymecha	N	M09-3.3	101.239°E 70.741°N	Pravoboyarsky Suite. Dense, strongly lithified 8-m-thick lapilli tuff. Altered, formerly glassy fragments. Major, areally extensive unit. (mj)	90% juvenile, 10% accidental.	Some altered, formerly glassy material fragments are highly vesicular, and apparently deformed by flow or compaction. Other fragments are poorly vesicular.	N/A
	X	M09-12.1	100.636°E 70.811°N	Delkansky Suite. Welded rhyolitic tuff. Purple-gray with feldspar laths. 10–20 m thick. (eLT)	95% juvenile, 5% accidental.		N/A
Nizhnyaya Tunguska		NT12-1	100.505°E 64.172°N	1-m-thick accretionary lapilli–bearing basal lapilli tuff directly above Tungusskaya sedimentary rocks. (bLTal)		Rare, poorly vesicular, and irregular altered, formerly glassy material fragments.	N/A
	P	NT12-4.2	100.867°E 64.114°N	Clast-rich lapilli tuff. (ml)			Uniformly magnetized at all T.
Severnaya	Q	S10-2-5	90.768°E 66.414°N	Well-lithified gray-and-white volcaniclastic rock with large clasts (up to 3 cm) of heterogeneous igneous and sedimentary rock. Fine ashy matrix. (ml?)	80% juvenile, 20% accidental.		Randomly magnetized. Incoherent intraclast directions. Unknown overprint?
Noril'sk		N12-8.2	88.331°E 69.620°N	Morongovsky Suite lapilli tuff. 15–30 m in total thickness. Very abundant spheroidal accretionary lapilli. (bLTal)		Small, equant, altered, formerly glassy material fragments.	N/A

Note: Componentry is estimated from thin section analyses and visual inspection of field photographs and outcrops. See Figures 1 and 2 for sampling locations.

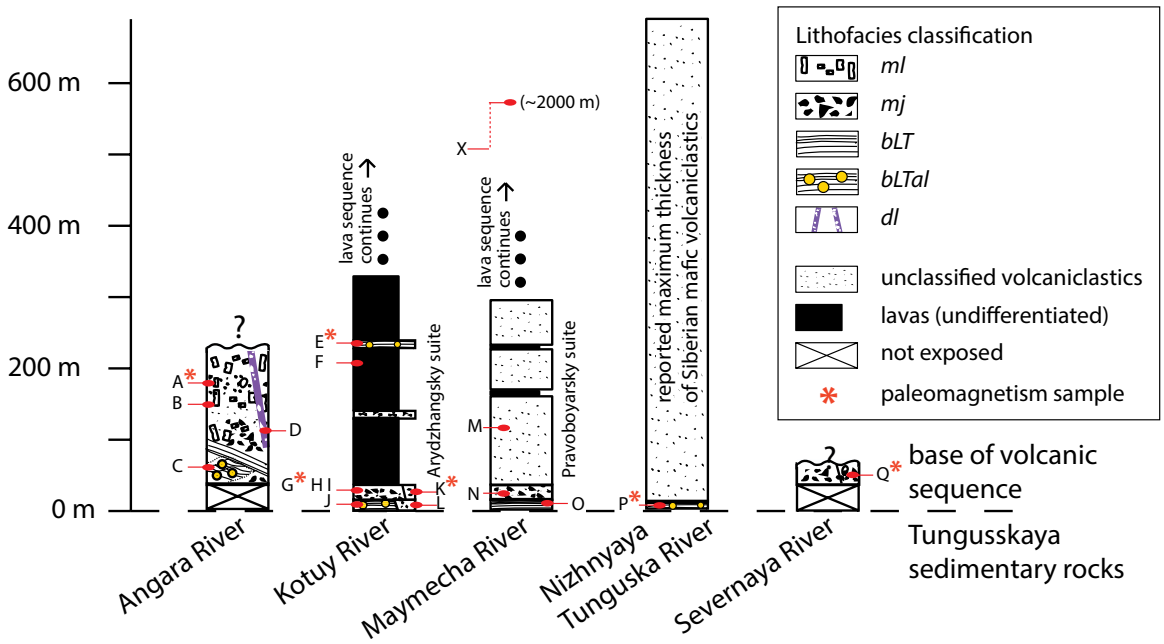

Figure 2. Stratigraphic sections of basal volcaniclastic and lava sequences of the Siberian Traps, based on Fedorenko et al. (2000), White et al. (2009), and our own observations. Thicknesses are laterally variable. Noril'sk is not shown because volcaniclastic layers are intercalated with lava flows. Letters denote units as follows: A—A10-A9B (paleomagnetism sample) and A10–7.1; B—A10–3.5; C—A10–13.3; D—A10–10.2; E—K08–11.6 (paleomagnetism sample); F—perovskite-bearing flow dated to 251.7 ± 0.4 Ma by Kamo et al. (2003); G—K08–7.11 (paleomagnetism sample); H—K08–7.10; I—K08–3.4; J—K09–7.7; K—K08–10.3 (paleomagnetism sample); L—K09–10.4A; M—volcaniclastic sequence described by Fedorenko et al. (2000), including "agglomerated tuffs"; N—M09–3.3; O—basal bLT with plane-parallel stratification and sand-wave bed forms; P—NT12–4.2 (paleomagnetism sample); Q—S10–2.5 (paleomagnetism sample); X—welded rhyolitic tuff from Delkansky Suite (~1700 m above top of Pravoboyarsky Suite shown here), dated to 251.17 ± 0.3 Ma by Kamo et al. (2003). Sampled units are described in more detail in Table 2. The contact with Permian sedimentary rocks at the base of the Angara and Severnaya River sections is covered, and erosion has removed the overlying stratigraphy. The volcaniclastic rocks of the Maymecha and Kotuy Rivers are capped by thick lava sequences (not shown here). The reported maximum thickness of the volcaniclastic rocks is based on drill core from near the center of the Tunguska Basin (Levitan and Zastoina, 1985; Zolotukhin and Almukhamedov, 1988). See Figure 3 for lithofacies descriptions.

magnetite (580 °C for pure Fe_3O_4) but higher than any postemplacement thermal conditions, clasts should contain two NRM components, assuming no subsequent overprinting (Hoblitt and Kellogg, 1979). The maximum blocking temperature of the unidirectional component is then a measure of the emplacement temperature. Information about emplacement temperatures can in turn correlate with distance from the vent (McClelland et al., 2004) and can help to differentiate rocks that originated in pyroclastic density currents from the lithified deposits of lahars and debris flows (Hoblitt and Kellogg, 1979). We do not apply a cooling rate correction (McClelland et al., 2004), because the thickness of individual layers is often difficult to determine.

We subjected clasts from six parent blocks to paleomagnetic analysis: K08–7.11, K08–10.3, K08–11.6, A10-A9B, S10–2.5, and NT12–4.2 (see Figs. 1 and 2 for geographic distribution and stratigraphic positions). Sample A10-A9B is composed of individual oriented bombs from site A9B of Latyshev et al. (2013). In addition to the basaltic (and in some cases sedimentary) clasts contained within these samples, K08–11.6 also hosts abundant accretionary lapilli.

Paleomagnetic measurements for samples K08–7.11, K08–10.3, K08–11.6, S10–2.5, and NT12–4.2 were acquired in the Massachusetts Institute of Technology (MIT) Paleomagnetism Laboratory. For these samples, we obtained paleomagnetic emplacement temperatures from the Siberian Traps volcaniclastic rocks by extracting mutually oriented 0.5–2 cm clasts from unoriented parent samples. Most samples were subjected to low-amplitude alternating frequency (AF) demagnetization (to 10 mT) to remove any viscous remanent magnetization or isothermal remanent magnetization associated with exposure to magnetic fields at ambient temperatures. We then measured the samples with a 2G Enterprises Superconducting Rock Magnetometer in combination with stepwise thermal demagnetization (increments of 15 °C to 50 °C) in an ASC Scientific TD48-SC oven housed in a magnetically shielded (<200 nT direct current [DC] field) room. Hysteresis data were collected with the vibrating sample magnetometer in the laboratory of C. Ross in the MIT Department of Materials Science and Engineering. Sample A10-A9B is the only oriented sample included in this study. Paleomagnetic measurements of A10-A9B were performed in the Petromagnetic Laboratory at Moscow State University and in the Laboratory of the Main Geomagnetic Field and Rock Magnetism of the Institute of Physics of the Earth (Russian Academy of Sciences) with JR-6 Spinner magnetometers, as described in Latyshev et al. (2013). In total, we measured >100 clasts from six samples, searching for a thermal overprint associated with emplacement of the samples.

RESULTS

Field Evidence

Based on bedding thickness and structures, grain size, sorting, componentry, and clast shapes, we classify the observed Siberian Traps volcaniclastic rocks into six distinct lithofacies. Because we have visited just a fraction of the localities where volcaniclastic rocks may be present, these lithofacies likely represent only a subset of the overall diversity of the volcaniclastic rocks. We describe our lithofacies next (sorted in rough order of decreasing prevalence in the areas we visited) and also provide summaries in Tables 1 and 2.

Lithofacies mj

Lithofacies mj (Fig. 3A) is composed of massive, poorly sorted tuff, lapilli tuff, or tuff breccia (lapilli tuff is most common, followed by tuff breccia) with primarily juvenile clasts and fine- to medium-grained ash matrix. These volcaniclastic rocks contain abundant mafic clasts 1–50 cm in diameter. They comprise layers reaching approximately 10 m thick on the Maymecha River within the Pravoboyarsky Suite (at the base of the volcanic section in the Maymecha region). Layers are typically internally structureless, but they may be bracketed by lavas and gradational or sharp contacts with ul, bLT, or bLTal layers. On the Maymecha River, mj rocks contain angular to fluidal mafic igneous clasts, flat-lying clasts, and occasional clast imbrication. Angular sedimentary clasts (1–5 cm in diameter) do exist in the rocks of the Pravoboyarsky Suite, but they are entirely absent in intercalated mj layers higher in the Maymecha and Kotuy sections.

Lithofacies ml

Lithofacies ml (Fig. 3A) is composed of massive tuff, lapilli tuff, or tuff breccia (lapilli tuff and tuff breccia are most common) with abundant, poorly-sorted lithic clasts with fine- to medium-grained ash matrix. The distribution of these lithic-rich rocks includes the Kotuy, Angara, and Nizhnyaya Tunguska River regions (Fig. 1). Thicknesses reach more than 200 m along the Angara River and ~30 m on the Kotuy River (Fig. 2), though in the Angara region, it can be challenging to distinguish rocks of the ml lithofacies from bLT rocks with faint, poorly developed beds. Angular to rounded clasts in an ml layer on the Kotuy River (sample K09–10.4A) include coal and siltstone fragments up to 50 cm in diameter (more typically <20 cm); angular clasts in Angara River outcrops include distinctive white limestone and sandstone up to 1 m in diameter (Fig. 3A), along with both fine-grained and medium-grained mafic igneous fragments (the medium-grained clasts are likely lithics, but the fine-grained, weakly vesicular clasts may be juvenile). On the Kotuy River, ml rocks unconformably overlie Permian sedimentary rocks. Svensen et al. (2009) have described the fragmental material, including altered mafic blocks and fragments of evaporate, that fills diatreme structures throughout the Tunguska Basin. These fragmental rocks may also belong to the ml or mj lithofacies.

Lithofacies bLT

Lithofacies bLT (Figs. 3B and 3C) is composed of bedded tuff and lapilli tuff (lapilli tuff is most common) characterized by 1–100-cm-thick beds with angular lapilli-sized juvenile and minor lithic clasts (locally imbricated) within fine- to medium-grained ash matrix. Bedding is commonly plane-parallel, though sand-wave bed forms are present in the Maymecha region. Thinly bedded (1–5 cm) layers occur in packages with thicknesses of 1 to 8 m, occurring near the base of the volcanic section on the Maymecha and Kotuy Rivers (Fig. 2). More thickly and faintly bedded layers, which can be difficult to distinguish from massive ml rocks, crop out on the Angara River (Fig. 3C): These rocks are poorly sorted, with shallowly dipping beds of 50–100 cm thickness.

Lithofacies bLTal

Lithofacies bLTal is composed of bedded tuff and lapilli tuff with accretionary lapilli (Figs. 3D and 3E). The thinly to thickly bedded fine tuff to lapilli tuff (beds tend to be 1–10 cm thick) usually display good sorting. Accretionary lapilli range in diameter from 1 mm to 30 mm and include discoidal, spherical, armored, rim-type, and multilayered morphologies (Fig. 4). Blocks and bombs are rare. Some bLTal rocks on the Angara River include thin beds consisting primarily of accretionary lapilli; these beds contain low-angle cross-stratification and normal grading. Bedded layers of lapilli tuff with accretionary lapilli also occur within the Morongovsky Suite, ~1000 m above the base of the Noril'sk volcanic section (Rudakova and Krivolutskaya, 2009). Fedorenko (1994) and Fedorenko et al. (1996) suggested that these rocks may be coeval with the Noril'sk-1 intrusion, which has a zircon age that overlaps within uncertainty with the onset of the mass extinction (Kamo et al., 2003; Burgess, 2014; Burgess et al., 2014).

Lithofacies eLT

Lithofacies eLT (Figs. 3F and 3G) is composed of eutaxitic tuff and lapilli tuff. The eLT rocks occur only as 1–10 m layers within the late-stage Delkansky Suite on the Maymecha River. These rhyodacitic and rhyolitic rocks are among the most silicic volcanic products of Siberian Traps magmatism (Fedorenko and Czamanske, 1997), and they crop out as distinctive purple- or red-colored layers within the sequence of mafic lavas with which they are intercalated (Fig. 3F). They often include crystals and crystal fragments 0.1–3 mm in length and small pumice fragments.

Lithofacies dl

Lithofacies dl is represented by volcaniclastic dikes with abundant lithic clasts (Figs. 3H and 3I); these dikes have ash- to lapilli-sized basaltic and sedimentary fragments, typically 30 cm to 1 m in thickness. Where observed in Angara outcrops, these dikes crosscut ml and bLT units and can reach >100 m in height.

Petrography and Geochemistry

We examined the volcaniclastic rocks in thin section with a petrographic microscope and an electron microprobe. Possibly because of their relatively high porosity and original glass contents, the volcaniclastic rocks are particularly vulnerable to secondary alteration (Büchl and Gier, 2003). Nonetheless, many primary volcanic features are preserved. The shape and vesicularity of formerly glassy fragments, which provide information about the fragmentation mechanism (Heiken, 1972; Wohletz, 1983), are listed in Table 2. The approximate proportion of juvenile and lithic particles is also given in Table 2.

Altered formerly glassy shards vary from sample to sample even within lithofacies, ranging from blocky grains (Heiken, 1972) with mosaic cracks (Büttner et al., 1999) and negligible vesiculation to highly vesicular, irregularly shaped fragments (Fig. 4E; Wohletz, 1983). Some smaller ash particles have moss-like shapes (Wohletz, 1983). Because most of the formerly glassy fragments are altered, however, some of these cracking patterns may postdate the original quenching of the glass.

Figure 4F shows fine-grained material that appears to have armored a small, equant, unvesiculated altered glass fragment. Generally, thin sections of accretionary lapilli revealed fine-grained rims and inwardly increasing ash grain size. The maximum grain size at the cores of accretionary lapilli (except for armored accretionary lapilli) is ~300 μm.

While it can be difficult to differentiate true juvenile from cognate fragments, the components of volcaniclastic rocks in Table 2 range from ~50% to 100% juvenile material and from 0% to 50% lithic material (excluding the clastic dikes, which can include even larger proportions of sedimentary material).

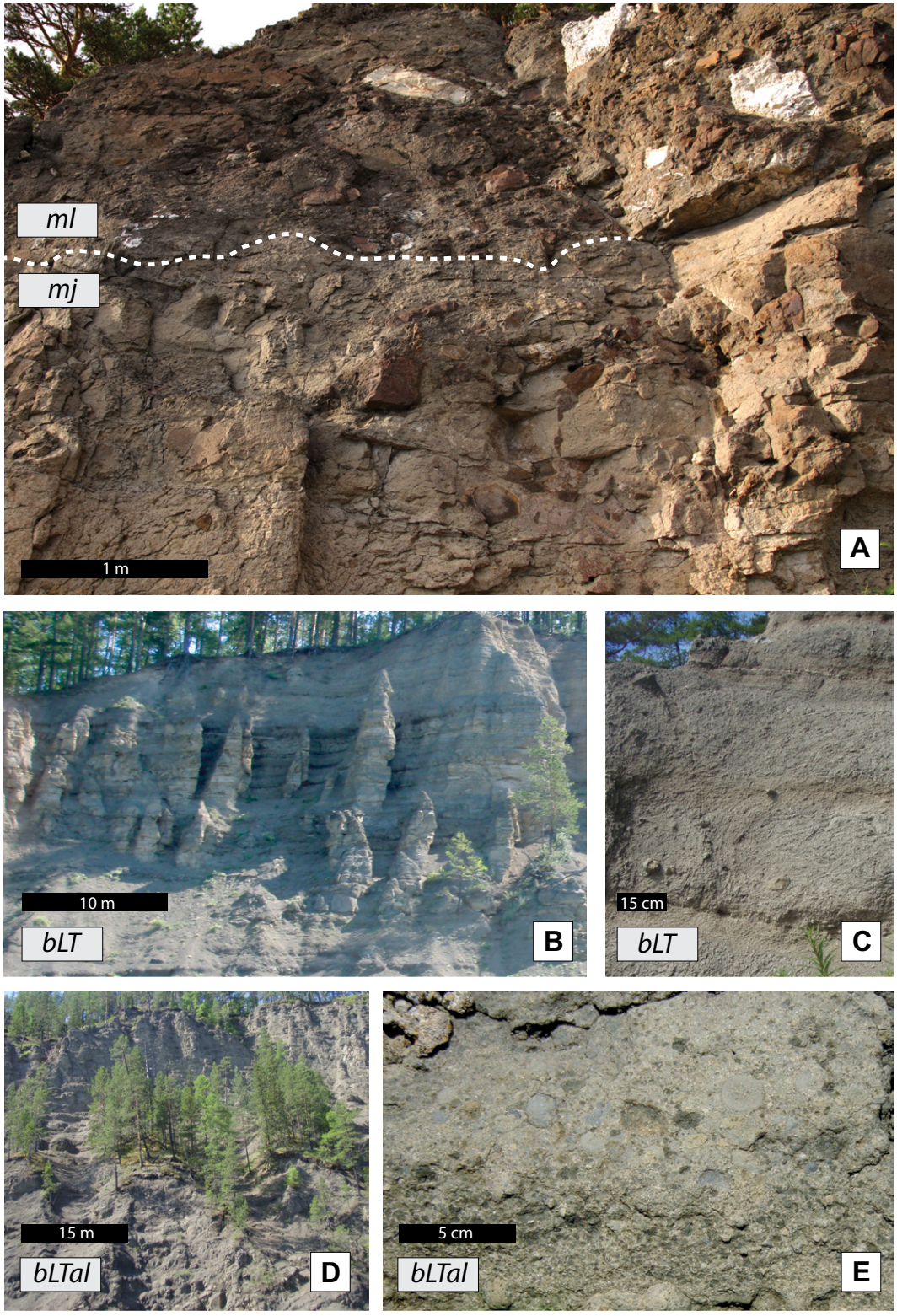

Figure 3 (*on this and following page*). Examples of Siberian Traps volcaniclastic lithofacies as described in Table 1. (A) Lithofacies ml with poorly sorted lapilli tuff and tuff breccia containing abundant lithic clasts (including stromatolitic limestone blocks), overlying mj lithofacies with poorly sorted lapilli tuff and tuff breccia with predominantly juvenile clasts (samples A10–7.1 and A10-A9B). (B) Lithofacies bLT, with shallow-dipping beds of lapilli tuff including both lithic and juvenile clasts (in the Angara region). (C) Close-up view of bLT rocks on the Angara River, with abundant angular basaltic clasts. (D) Outcrop on the Angara River with abundant bLTal beds (shown in E) near the base of the cliff; rocks near the top of the cliff were not accessible, and hence their lithofacies are uncertain. (E) Lithofacies bLTal: accretionary lapilli–bearing lapilli tuff with thin planar beds (low-angle cross-stratification is also present in the same outcrop). Sample A10–13.3.

Because of the large quantity of accidental material incorporated into many of the volcaniclastic rocks, whole-rock geochemical analyses often do not reflect the composition of the magma. The available geochemical data show that the juvenile materials in Siberian Traps volcaniclastic rocks are predominantly basaltic (with the exception of the silicic eLT rocks; Sharma, 1997). Fedorenko et al. (2000) and Fedorenko and Czamanske (1997) presented whole-rock geochemistry for the volcaniclastic rocks in the Maymecha and Kotuy regions, and Black et al. (2012) presented melt inclusion data.

Heunemann (2003) has characterized the petrography of Siberian Traps basalts with an

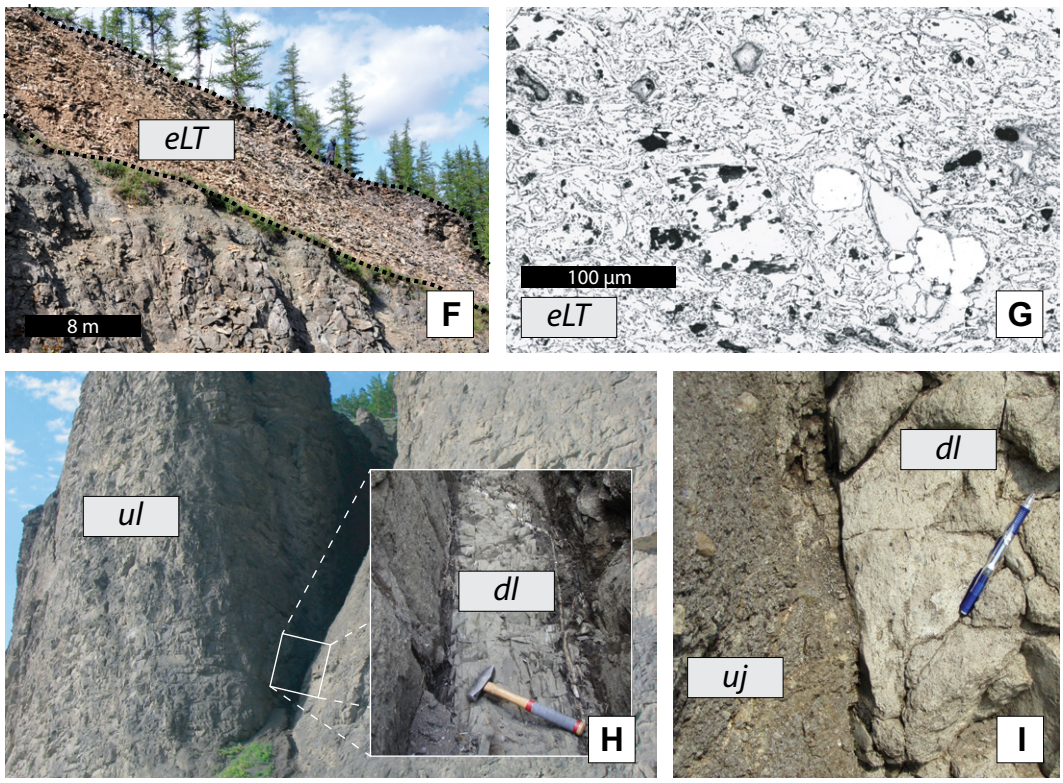

Figure 3 (*continued*). (F) Lithofacies eLT rhyodacitic tuff in the Maymecha River region. (G) Reflected light image of eLT rhyolitic tuff in thin section showing eutaxitic texture and broken crystal fragments (sample M09–12.1). (H) Volcaniclastic dike (dl) with abundant juvenile and lithic fragments crosscutting a 100 m cliff of predominantly ml lithofacies lapilli tuff (Angara region, hammer for scale). (I) Close-up view of the subvertical contact between a volcaniclastic dike (dl) and mj rocks (Angara region).

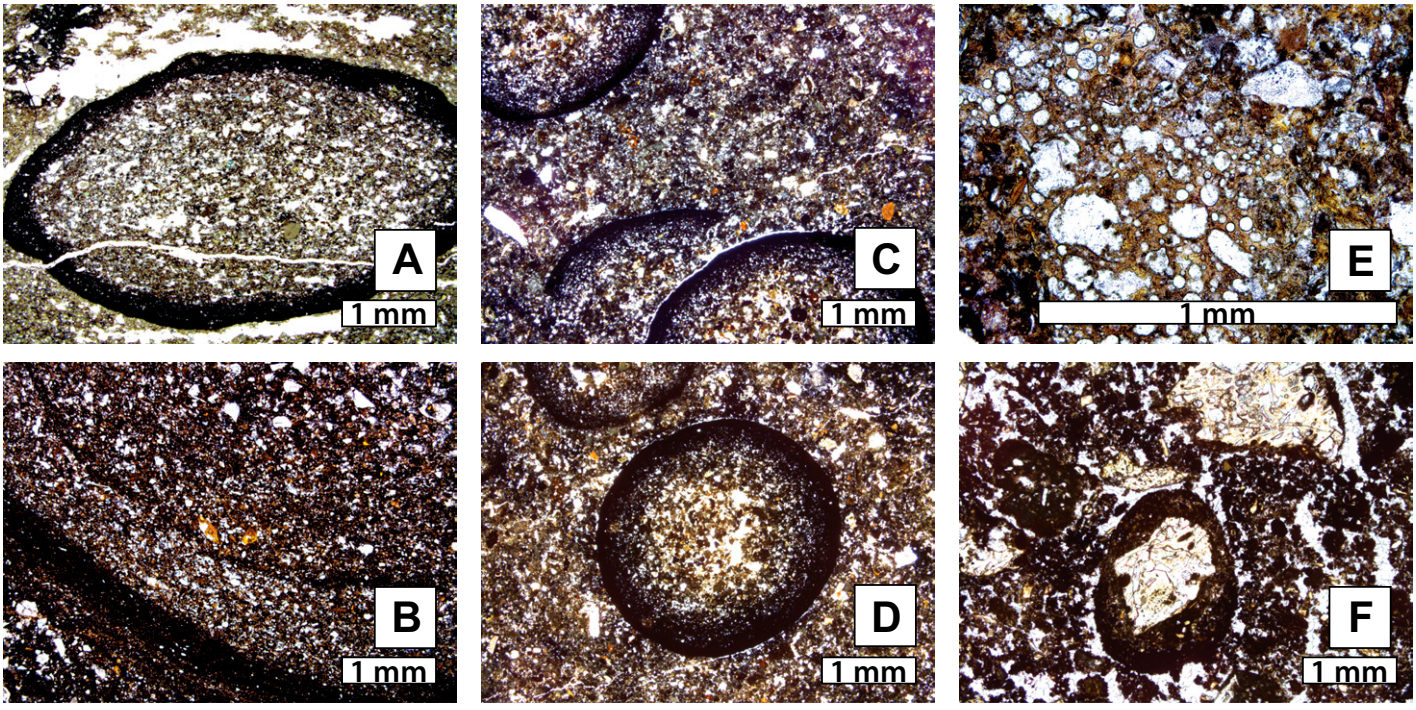

Figure 4. Petrographic images of volcaniclastic rocks in thin section, taken with plane-polarized light source. (A) Rim-type oblate accretionary lapillus in lowermost Nizhnyaya Tunguska lapilli tuff (sample NT12–1). (B) Multilayered large accretionary lapillus with grain size increasing toward core (sample A10–13.3). (C) Abundant spherical accretionary lapilli from Morongovsky lapilli tuff in Noril'sk (sample N12–8.2). There are numerous broken fragments of accretionary lapilli within this sample, as shown by the partial rim center left. (D) Well-preserved rim-type spherical accretionary lapilli from Morongovsky lapilli tuff (sample N12–8.2). (E) Small fragment of highly vesicular, formerly glassy fragment from Pravoboyarsky mj lapilli tuff (sample M09–3.3). (F) Fine-grained material armoring an equant, poorly vesicular altered originally glassy fragment (sample K09–11.6).

emphasis on the magnetic minerals. He reported titanomagnetite/ilmenite intergrowths in lavas from Noril'sk, indicating primary high-temperature oxidation of grains that would not interfere with the fidelity of the rocks as magnetic recorders (Heunemann, 2003). The magnetic mineralogy of Siberian Traps rocks, and of our samples in particular, is discussed in further detail in the following section.

Paleomagnetism

Previous paleomagnetic studies of the Siberian Traps have identified magnetite and titanomagnetite as the primary carriers of magnetic remanence, with grains predominantly in the pseudo-single-domain size range (Gurevitch et al., 2004; Lind et al., 1994; Pavlov et al., 2007). The magnetization components we identified provide additional context for the mineralogy of our samples (these components are described in more detail in the next paragraph). While the >585 °C component in two clasts from K08–11.6 suggests that hematite is present in this sample, the peak 585 °C unblocking temperature of the NRM for most clasts of K08–11.6 (GSA Data Repository Fig. A1[1]) is consistent with near-stoichiometric magnetite as the major NRM carrier. In addition to magnetite, K08–7.11 and NT12–4.2 both appear to host a mineral with a Curie temperature close to 300 °C, which is likely titanomagnetite (Kazansky et al., 2005; Pavlov et al., 2011). Curie temperatures of titanomagnetite may depend on mineral composition and oxidation history (Dunlop and Özdemir, 2001). Heunemann (2003) has argued that titanomagnetites from Noril'sk lavas experienced high-temperature oxidation. In that case, a Curie temperature of ~300 °C would correspond to titanomagnetite with a composition close to $Ti_{0.45}Fe_{2.55}O_4$ (Dunlop and Özdemir, 2001; Schult, 1970). Such a composition is more Ti-enriched than that of $Ti_{0.2}Fe_{2.8}O_4$ titanomagnetites from near Noril'sk (Heunemann, 2003), consistent with the large number of high-Ti lavas endemic to the Maymecha-Kotuy region (Fedorenko et al., 2000). Our hysteresis data for clasts from K08–10.3 and K08–7.11, including the ratio of saturation remanence to saturation magnetization (M_{rs}/M_s) and the ratio of remanent coercive force to ordinary coercive force (H_{cr}/H_c) for K08–7.11 (GSA Data Repository Fig. A2 [see footnote 1]), indicate that as found in previous studies (Gurevitch et al., 2004; Lind et al., 1994; Pavlov et al., 2007), the ferromagnetic minerals are predominantly in the pseudo-single-domain size range (Dunlop, 1990). During our optical and electron microprobe investigations, we did not identify any ferromagnetic minerals, consistent with a relatively fine (pseudo-single-domain) grain size.

The results from stepwise thermal demagnetization of our samples are shown in Figures 5 and 6 (for clarity, AF demagnetization steps are not shown here, but are plotted separately in GSA Data Repository Fig. A3 [see footnote 1]). We used principal component analysis (Kirschvink,

[1]GSA Data Repository item 2015161, Additional details of paleomagnetic analyses and the complete set of unprocessed paleomagnetic data, is available at http://www.geosociety.org/pubs/ft2015.htm or by request to editing@geosociety.org.

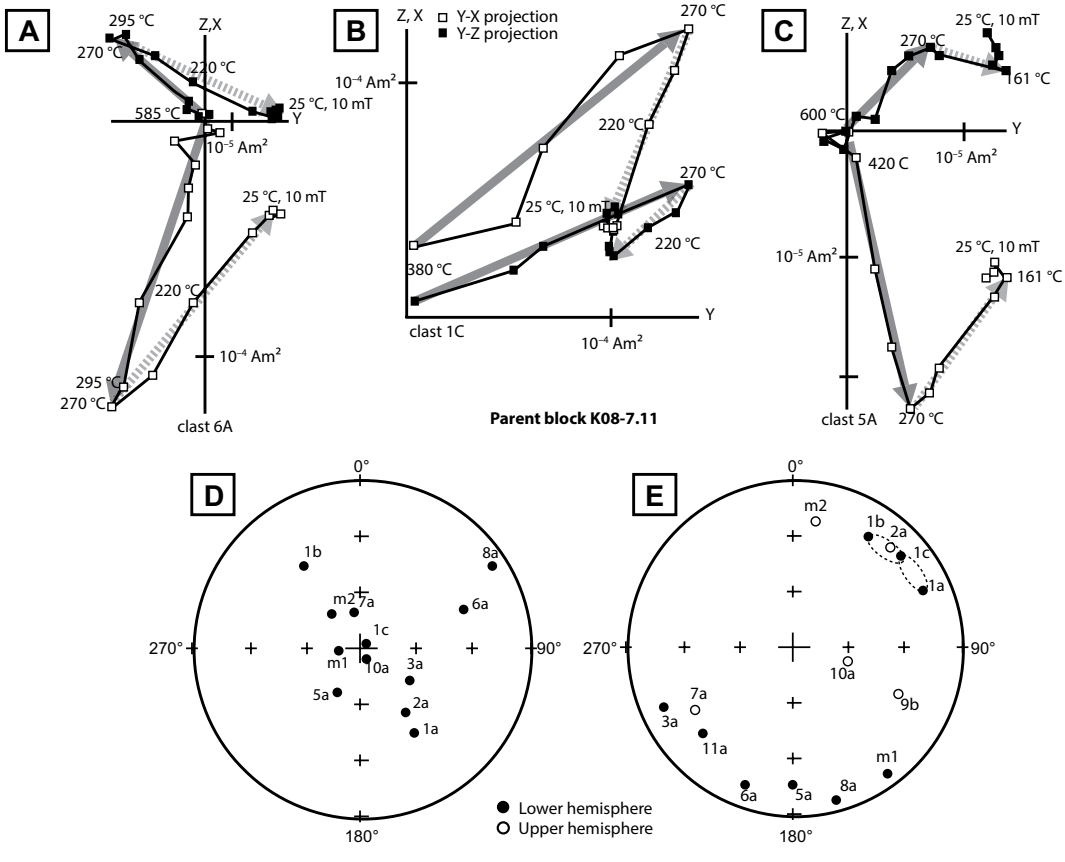

Figure 5. Paleomagnetic results from clasts from parent block K08–7.11, a mafic lapilli tuff from the Kotuy River valley. Because the sample is not absolutely oriented, all directions are oriented relative to an arbitrary coordinate system fixed to the parent sample and not geographically. (A–C) Orthographic projection showing the natural remanent magnetization (NRM) of selected clasts from K08–7.11 during stepwise thermal heating. Open symbols indicate projection onto the horizontal plane; closed symbols indicate projection onto the vertical plane. Most clasts reveal two components: an low-temperature (LT) component (light dashed arrows) blocked up to ~270 °C and a high-temperature (HT) component (dark shaded arrows) blocked up to >270–330 °C. Alternating frequency (AF) demagnetization for these clasts is shown in GSA Data Repository Figure 3 (see text footnote 1). (D) Equal-area stereographic projections showing nonrandomly oriented LT component directions in individual clasts (resultant $R > R_{95\%}$, where $R_{95\%}$ is the critical resultant at 95% confidence). Open and closed symbols denote upper and lower hemispheres, respectively. (E) Equal-area stereographic projection showing HT directions for which randomness cannot be rejected at the >95% confidence interval ($R < R_{95\%}$). Individual clasts are labeled. Subsamples from the same clast are linked with dotted circles.

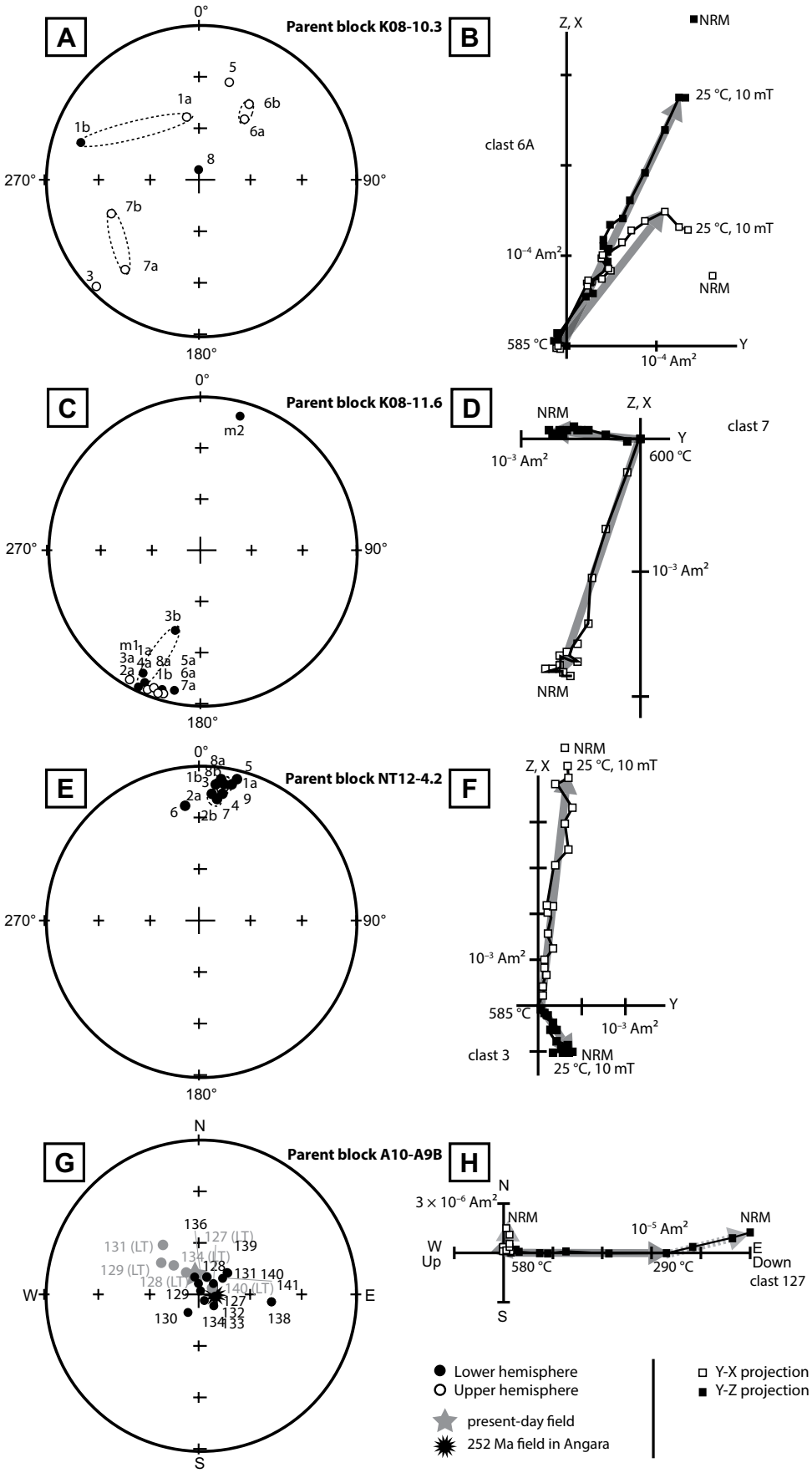

Figure 6. Equal-area stereographic projections (left column) and orthographic projections (right column) showing component directions in clasts from parent blocks K08–10.3, K08–11.6, NT12–4.2, and A10-A9B. In stereographic plots, open and closed circular symbols denote upper and lower hemispheres, respectively. In orthographic plots, open square symbols indicate projection onto the horizontal plane, and closed symbols indicate projection onto the vertical plane; dark shaded arrows denote high-temperature (HT) components, and light dashed arrows denote very low-temperature (VLT) components. Because samples in A–F are not absolutely oriented, their directions are given relative to an arbitrary coordinate system fixed to the parent sample and not geographically. (A) HT components from sample K08–10.3, interpreted as a conglomerate produced by a lahar or debris flow. (B) Zijderveld (orthographic) projection of remanent magnetization of clast 6A from sample K08–10.3 during stepwise heating. Many clasts in this parent block display complex behavior that differs from clast to clast. In this clast, the demagnetization has a low-temperature curvature and may retain a component at >585 °C. (C) Sample K08–11.6, a reddish accretionary lapilli–bearing rock, which is uniformly magnetized at low and high temperatures. (D) Zijderveld (orthographic) projection of remanent magnetization of clast 7 from sample K08–11.6 during stepwise heating; this clast was not subjected to alternating frequency (AF) demagnetization prior to heating. (E) Clast-rich NT12–4.2 displays a single, uniform component of magnetization. (F) Zijderveld (orthographic) projection of remanent magnetization of clast 3 from sample NT12–4.2 during stepwise heating. (G) A10-A9B is the only oriented sample and is consistent with an HT component overprinted by the present-day field. VLT component plotted in light gray; HT component in solid black. (H) Zijderveld (orthographic) projection of remanent magnetization of clast 127 from sample A10-A9B during stepwise heating. Sample A10-A9B was not subject to AF demagnetization prior to heating. NRM—natural remanent magnetization.

1980) to identify NRM components. We classified the components as very low temperature (VLT; when blocked from 50 °C to 210 °C), low temperature (LT; when blocked from 50 °C to 300 °C), high temperature (HT; when blocked from 50 °C to 585 °C), or very high temperature (VHT; when blocked above 585 °C, which applies to just two clasts from K08–11.6; GSA Data Repository Table A1 [see footnote 1]). Out of six parent samples, clasts from two (K08–11.6, and NT12–4.2) contain only a single coherent component of magnetization (with the exception of two K08–11.6 clasts that have HT and VHT components). Clasts from A10-A9B, K08–7.11, and K08–10.3 contain one or two components of magnetization. Clasts from S10–2.5 do not display coherent magnetizations within or across clasts.

We applied Watson's (1956) test to assess the randomness of the distribution of paleomagnetic directions. The resultant vector for a set of unit vectors oriented in the clast NRM directions is compared to a critical value at the 95% level ($R_{95\%}$). If $R > R_{95\%}$, the clasts are nonrandomly magnetized, and the test is considered "failed." Conversely, if $R < R_{95\%}$, then we cannot reject randomness at the 95% confidence level, and the test is considered "passed."

The Watson test results for all components for each sample are listed in GSA Data Repository Table A2 (see footnote 1). HT components from three samples (K08–11.6, NT12–4.2, and A10-A9B) fail the conglomerate test ($R/R_{95\%} > 1$) and so contain nonrandomly oriented magnetization (representative orthographic projection for K08–11.6 is shown in Fig. 6B). Both LT and HT components from sample K08–10.3 pass the test ($R/R_{95\%} < 1$, as noted in Fig. 6A). S10–2.5 contains clasts with internally inconsistent and unstable magnetization, and so the conglomerate test for this sample is inconclusive. The LT component of K08–7.11 fails the conglomerate test ($R/R_{95\%} > 1$, as noted in Fig. 5D), while the HT component passes ($R/R_0 < 1$, as noted in Fig. 5E). The majority of the clasts from this final sample exhibit a sharp directional change in the demagnetization path around 270 °C (Figs. 5A–5C), although two clasts (9b and 11a) contain only a single component up to the blocking temperature of magnetite. Where possible, we subsampled large clasts to check the consistency of intraclast magnetization. With the exception of S10–2.5, all samples displayed homogeneous directions within clasts.

DISCUSSION AND INTERPRETATION

Interpretation of Volcaniclastic Lithofacies

While uniquely diagnostic features are often absent from Siberian Traps volcaniclastic rocks, many rocks do preserve sets of characteristics that in combination are most consistent with particular genetic interpretations. Here, we outline our preferred interpretations based on the attributes of each of our proposed lithofacies.

Lithofacies mj: massive tuff, lapilli tuff, or tuff breccia with primarily juvenile clasts. These rocks are the most difficult to interpret based on textural observations alone. We interpret thin layers of mj rocks with negligible ash that are intercalated with lavas as either brecciated flow bottoms and flow tops or as the products of magmatic fire fountaining (these alternatives could be tested with further mapping). We interpret mj rocks in the Kotuy and Angara regions that contain overwhelmingly juvenile clasts (in particular, clasts with glassy rinds) separated by ashy matrix as possible hyaloclastites. Because massive hyaloclastites should be spatially associated with subaqueous lavas, future identification of nearby pillowed flows or pillow fragments would buttress this interpretation. Some mj rocks in the Maymecha and Angara regions, especially those that underlie or overlie ml or bLT lithofacies (Fig. 3A), may also result from pyroclastic density currents.

Lithofacies ml: massive tuff, lapilli tuff, or tuff breccia with abundant lithic clasts. The poor sorting, rarity of fabrics, and presence of large blocks in ml rocks could be consistent with original deposition by lahars or pyroclastic density currents (Ross and White, 2005). In one outcrop on the Angara River, we observed a set of lenticular beds (each ~10 cm thick and 1–2 m wide) with abundant well-rounded 2–5 cm gravel (both igneous and sedimentary) and high-angle truncation surfaces. These features are consistent with fluvial activity (and imply that there was a source of erodible country rock nearby and that the Angara region was not fully submerged at the time the volcaniclastic rocks were emplaced) and are markedly different from the ml rocks. Most ml layers are very poorly sorted, without channeling, rounded clasts, or high-angle cross-stratification, arguing against a fluvial origin (Ross and White, 2005). It is more difficult to identify or rule out deposition by lahars. The ml rocks often contain altered glass fragments, abundant lithic clasts from specific sedimentary layers apparently not exposed near the surface (such as the white stromatolitic limestone in Fig. 3A), angular upright blocks, and rare composite bombs with sedimentary rocks armored by igneous material. While these features do not conclusively exclude transport in lahars, they are more consistent with phreatomagmatic pyroclastic density currents.

Lithofacies bLT: bedded tuff and lapilli tuff. We suggest that these rocks originated in subaqueous or subaerial density currents. Shallowly dipping beds in the Angara region (Fig. 3B) resemble deposits in Iceland, Japan, and the Faroe Islands that have been interpreted as hyaloclastite foresets (Yamagishi, 1991; Bergh and Sigvaldason, 1991; Jerram et al., 2009). However, the high abundance of sedimentary clasts in the Siberian rocks and the rarity of pillow fragments are atypical for bedded hyaloclastites (Yamagishi, 1991). In some outcrops on the Angara River, bLT rocks include charcoalized woody fragments ~10 cm in length. Because the Siberian Traps erupted in a continental basin rather than a submarine setting (Czamanske et al., 1998), we suggest that shallow surface water encouraged a hybrid or changing eruption style that included episodes of proximal hyaloclastite formation and episodes of phreatomagmatic explosivity. Subaqueous and pyroclastic density currents resulting from these two eruption modes could both produce bLT volcaniclastic rocks.

Lithofacies bLTal: bedded tuff and lapilli tuff with accretionary lapilli. This lithofacies includes many of the best-sorted and most texturally rich volcaniclastic rocks in the areas of the Siberian Traps we visited. While plane-parallel stratification is most common, some beds are cross-stratified at low angles or contain sand waves. As with most ul, uj, and bLT layers, the absence of channelization and high-angle cross-stratification, and the rarity or absence of rounded clasts argue against a fluvial origin. Taken together with the presence of well-preserved and often abundant accretionary lapilli (which typically coalesce in water-rich, turbulent eruption columns; Schumacher and Schmincke, 1995), the bed forms are most consistent with deposition by moist, dilute pyroclastic density currents. While such density currents are not unique to phreatomagmatic eruptions, many bLTal rocks (particularly in the Angara region) also contain high proportions of lithic material. We interpret these lithic-rich bLTal rocks as the products of phreatomagmatically derived dilute pyroclastic density currents. Because exposures showing relationships with preexisting topography are limited, we do not exclude the possibility that some bLTal rocks also originated as fallout deposits.

Lithofacies eLT: eutaxitic tuff and lapilli tuff. The eutaxitic texture suggests these well-sorted, fragmental silicic tuffs were emplaced while still hot by pyroclastic density currents.

Lithofacies dl: volcaniclastic dikes with abundant lithic clasts. The subvertical contacts and crosscutting relationships indicate these dikes postdate the surrounding volcaniclastic rocks. The mixtures of lithic and juvenile clasts suggest these originated from interactions between magmas and wet sedimentary material.

Interpretation of Paleomagnetic Results

Paleomagnetic data can provide insights into likely formation mechanisms for volcaniclastic rocks (such as those belonging to the mj and ml lithofacies) where the volcanological evidence is inconclusive. Because lahars and epiclastic deposits should be emplaced at temperatures less than 100 °C, and because juvenile fragments that were initially moving while cooling should not retain a random HT component (McClelland et al., 2004), our paleomagnetic data allow us to positively identify hot-emplaced pyroclastic rocks. Depending on the behavior of clasts from each sample during stepwise thermal demagnetization, we attempted to differentiate the original conditions under which the sample acquired its remanence. Figure 7 summarizes the framework within which we interpreted our paleomagnetic results.

Clasts from sample K08–7.11 (lithofacies uj) contain nonrandom LT and random HT components (Figs. 5D–5E). We interpret this paleomagnetic behavior as a record of emplacement at ~270 °C, consistent with pyroclastic eruption.

Sample A10-A9B (lithofacies ul), our only oriented sample, hosts a VLT component. While mean paleomagnetic direction for the Angara region at 252 Ma is very similar to the direction of the present-day field (Latyshev et al., 2013), the present-day field direction lies within the 95% confidence angle of the VLT component, whereas the 252 Ma field does not. The 95% confidence circles for the mean VLT and HT directions are very close, but they do not overlap. Given the VLT component's low (~200 °C) blocking temperature, we therefore interpret the VLT component in A10-A9B as a viscous remanent magnetization (VRM; Pullaiah et al., 1975). Unlike K08–7.11, both the VLT and HT components in A10-A9B fail the conglomerate test and are tightly clustered (Fig. 6H).

Sample K08–10.3 (lithofacies uj) passes the conglomerate test for both the LT and HT components with consistent intraclast directions. The unit from which we obtained this sample also discordantly cuts several lava flows. Accordingly, we conclude that K08–10.3 originated as a debris flow or lahar. This determination is consistent with the findings of Pavlov et al. (2011), who reported that clasts from another volcaniclastic layer sampled nearby also pass the conglomerate test.

Clasts from parent blocks K08–11.6 (lithofacies bLTal) and NT12–4.2 (lithofacies ul) each contain single unidirectional components of magnetization blocked to temperatures above the Curie point of magnetite that fail the conglomerate test. As mentioned above, the VLT and HT components in clasts from A10-A9B also fail the conglomerate test. These three samples are widely distributed across the Siberian Traps (Fig. 1). These results allow two possible interpretations: Either the samples were emplaced at temperatures greater than the blocking temperature of the high-temperature magnetic carrier, or they have been thermally or chemically overprinted after emplacement and primary cooling.

Several lines of evidence suggest that the Kotuy River volcaniclastic rocks (including sample K08–11.6) may record a primary magnetization from the time of emplacement. K08–11.6 is well lithified and contains millimeter- to centimeter-scale accretionary lapilli. Furthermore, two volcaniclastic samples collected several hundred meters away have passed the conglomerate test: sample K08–10.3 (reported here) and a nearby "tuff interlayer" (Pavlov et al., 2011), suggesting that these rocks have not been collectively overprinted. On the basis of this evidence, we conclude that the uniform HT component in K08–11.6 supports emplacement at greater than 580–600 °C, most likely associated with pyroclastic volcanism. This range of temperatures exceeds the emplacement temperatures expected for systems that incorporate abundant external water (Koyaguchi and Woods, 1996; McClelland et al., 2004), which contrasts with the presence of accretionary lapilli. We infer that the eruption that produced K08–11.6 incorporated relatively minor quantities of external water.

The evidence is more ambiguous for sample A10-A9B from the Angara River and sample NT12–4.2 from the Nizhnyaya Tunguska River. Neither sample is welded or sintered. However, the minimum temperature to incur welding of mafic materials may exceed the Curie temperature of magnetite (Sheridan and Wang, 2005), in which case deposition could occur at or above the Curie temperature without leaving textural evidence. Latyshev et al. (2013) reported statistically uniform directionality at the 95% confidence level among a subset of volcaniclastic rocks (including A10-A9B), dikes, and the Tolstomysovsky sill on the Angara River. Because other volcaniclastic rocks and intrusives retain HT components that are distinct from that of A10-A9B and the Tolstomysovsky sill at the 95% confidence level, and because Ordovician sedimentary rocks <1 km from the contact with the Tolstomysovsky sill have not been remagnetized, Latyshev et al. (2013) interpreted the directional groups as distinct primary magnetizations associated with rapid magmatic pulses that do not average secular variation. The balance of existing evidence thus suggests sample A10-A9B may have been emplaced at high temperatures. However, this conclusion is less certain than in the case of samples K08–7.11 and K08–11.6.

In the following section, we synthesize the volcanological evidence and these paleomagnetic constraints on emplacement temperatures to estimate the extent of Siberian Traps pyroclastic volcanism.

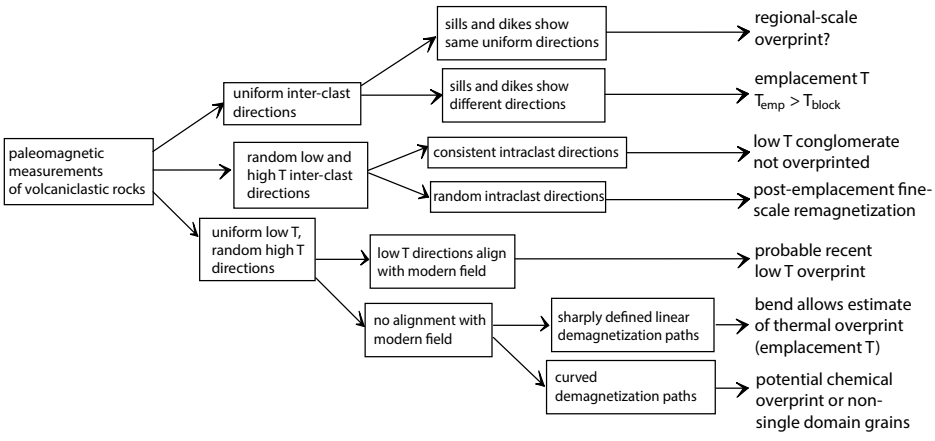

Figure 7. Flow chart showing potential implications of partial thermal demagnetization measurements of volcaniclastic rocks.

Extent of Pyroclastic Volcanism

Regardless of the origin of the volcaniclastic rocks associated with the Siberian Traps, pulses of particularly high magma flux likely resulted in fire fountaining and injection of gases into the lower stratosphere (Black et al., 2012; Glaze et al., 2015) accompanied by emplacement of flood basalt lavas. Because the Siberian Platform was located at ~60°N in the Permian (Latyshev et al., 2013), the mean altitude of the tropopause above the magmatic center was only ~10 km (Grise et al., 2010; Black et al., 2012),

though the precise altitude depends on atmospheric CO_2 levels (Held, 1982). Plume heights above fire fountains during large igneous province eruptions are expected to reach 13–17 km (Glaze et al., 2015). Exceptionally vigorous fire fountains during the historic Laki flood basaltic eruption produced columns that breached the tropopause (Thordarson and Self, 1993; Thordarson et al., 2003). The eruption of the Roza Member of the Columbia River Basalts probably generated kilometer-high fire fountains surmounted by convective plumes (Brown et al., 2014).

With this background in mind, in this work we focus on the volcaniclastic rocks. Why are there unusually large volumes of volcaniclastic rocks associated with the Siberian Traps, and do these rocks reflect unusually extensive explosive activity beyond the expected magmatic fire fountaining at vents?

We envision a diverse array of Siberian Traps eruptive styles (Fig. 8). We estimate that ~5%–10% of the volcaniclastic rocks we sampled fall into the bLTal lithofacies, which we interpret here as likely pyroclastic rocks (Table 1). A further ~20% of the volcaniclastic rocks belong to the bLT lithofacies, which we suggest includes both bedded hyaloclastites and lithified pyroclastic density current deposits. The ml and mj volcaniclastic rocks are massive, poorly sorted, and difficult to interpret texturally, and the dl and eLT rocks are volumetrically negligible.

Our paleomagnetic measurements and field and petrographic observations (Table 2) offer some additional constraints, in particular for the ml and mj rocks. As described in the previous section, we find evidence for one pyroclastic sample emplaced at ~270 °C (uj K08–7.11), one debris flow/lahar sample (uj K08–10.3), one sample with overprints or poor magnetic recording properties such that even intraclast directions are inconsistent (ul S10–2.5), one sample likely emplaced at temperatures above 580–600 °C (bLTal K08–11.6), and two samples emplaced either at temperatures above 580–600 °C or at unknown temperature and subsequently overprinted (ul A10-A9B and ml NT12–4.2). Thus, depending on how many of the uniformly magnetized samples all record hot emplacement, on the order of one sixth to two-thirds of the texturally ambiguous mj and ml Siberian Traps volcaniclastic rocks we analyzed may retain paleomagnetic evidence for emplacement during hot, pyroclastic eruptions.

Given the heterogeneity of Siberian Traps volcaniclastic rocks (Table 2), these results may be most directly relevant to the regions we visited (Fig. 1). We estimate the total area covered by our field work as the sum of L^2, where L is the length of each of our sampling transects. This estimated coverage area is ~100,000 km^2, compared to an original area of volcanic activity spanning ~3,000,000 km^2 (Reichow et al., 2009). If the mean thickness of volcaniclastic rocks is 200–300 m (Zolotukhin and Almukhamedov, 1988; Ross et al., 2005), the volume of volcaniclastic rocks in this coverage area is around 20,000–30,000 km^3. Any attempt to estimate the extent of pyroclastic volcanism incorporates considerable uncertainty in the volume of volcaniclastic rocks and the degree to which the paleomagnetic samples are representative. However, if we assume that our samples are representative and that in total ~30%–70% of the volcaniclastic rocks (across all lithofacies) result from explosive volcanism, we find a volume of pyroclastic rocks within the area covered by our field work of roughly 10,000 km^3.

Siberian Traps diatreme structures infilled with hydrothermally altered basaltic fragments are synchronous with volcanism (Svensen et al., 2009), and at least one diatreme actually crosscuts apparently related volcaniclastic rocks (Wooden et al., 1993). However, the largest diatremes have not been definitively linked with specific volcaniclastic layers. If the diatreme structures and a large fraction of the volcaniclastic rocks are in fact cogenetic, they represent a major phreatomagmatic province similar in style to that reported in the Transantarctic Mountains (McClintock and White, 2006; White and McClintock, 2001; Ross and White, 2005, 2006; Ross et al., 2008). Overall, the volcanological evidence for interactions between magmas and abundant external water supports the paleogeographic reconstructions of Czamanske et al. (1998), in which much of Siberia was water-logged in the latest Permian.

Effects on Gas Release and Environmental Consequences

Why do some large igneous provinces appear to coincide with mass extinctions, whereas others do not? The mafic volcaniclastic rocks of the Siberian Traps have been linked to unusually extensive explosive volcanism and to more pronounced environmental consequences (Campbell et al., 1992; Black et al., 2012). However, the correlation and potential causal links between the volume of volcaniclastic rocks and extinction severity are not clear. The Siberian Traps, Karoo-Ferrar (White and McClintock, 2001; Ross and White, 2005; McClintock and White, 2006; White et al., 2009), and Emeishan (Ross et al., 2005; Peate and Bryan, 2008; White et al., 2009; Wignall et al., 2009) large igneous provinces all contain significant volumes of mafic volcaniclastic rocks, whereas the Paraná-Etendeka, Central Atlantic magmatic province, and Columbia River provinces contain fewer volcaniclastic rocks. Of these, the Siberian Traps, Karoo-Ferrar, Emeishan, and Central Atlantic magmatic

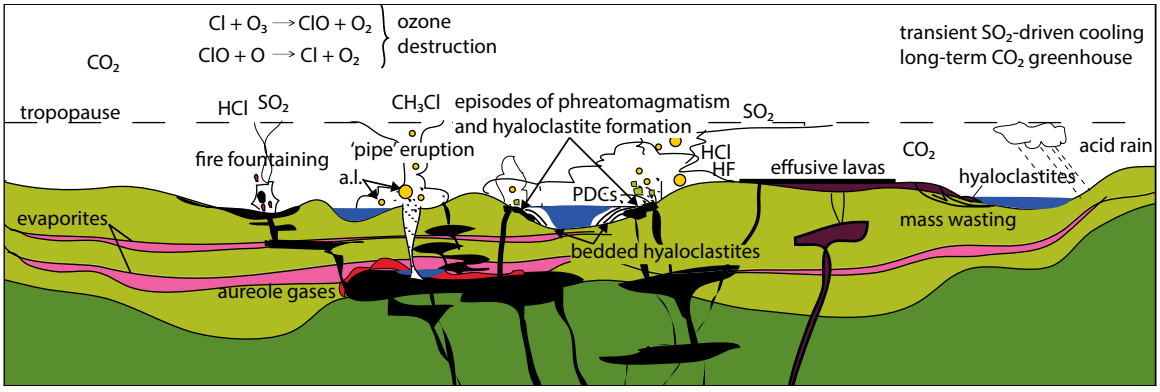

Figure 8. A schematic cross section through the upper crust and atmosphere during the Siberian Traps eruption (with emphasis on processes forming volcaniclastic rocks). Not to scale. PDCs—pyroclastic density currents; a.l.—accretionary lapilli.

province coincided with mass extinctions, within uncertainty, whereas extinction rates were low at the time of the Paraná-Etendeka and Columbia River eruptions (Wignall, 2001).

Our interpretations imply that the majority of the Siberian Traps volcaniclastic rocks originated through magma-water interactions. In the case of the subset of bLT, uj, and ml rocks that fragmented during interactions between lavas and surface water, the atmospheric consequences are likely minimal. In such a setting, the level of explosivity is typically low (Batiza and White, 2000), and the majority of volcanic degassing occurs near the vent (Thordarson and Self, 1998).

We also interpret some volcaniclastic rocks as the results of phreatomagmatic explosions. In certain regimes, phreatomagmatic explosivity may enhance the likelihood that a buoyant volcanic plume will develop (Koyaguchi and Woods, 1996). However, in the case of the Mawson Formation in the Ferrar large igneous province, Ross et al. (2008) argued that the coarseness of the deposits and the paucity of widespread ash-fall layers are consistent with subplinian eruption plumes generally <10 km in height, limiting the environmental consequences. Similarly, few continuous, extensive basaltic ash-fall layers have been identified in the Siberian Traps. If plume heights resulting from Siberian Traps phreatomagmatism did not reach stratospheric altitudes, most environmental effects from phreatomagmatic eruptions would have been regional in extent. While mapping any individual ash-fall layers would be challenging given the discontinuity and inaccessibility of many Siberian Traps outcrops, such an effort in the future could constrain column heights associated with Siberian Traps phreatomagmatism.

Hydrogen chloride is highly soluble in water and relatively soluble in water ice (Pinto et al., 1989; Tabazadeh and Turco, 1993; Textor et al., 2003). The additional water in a phreatomagmatic eruption plume would have expedited the rain-out of HCl (Tabazadeh and Turco, 1993; Black et al., 2012). Accordingly, magmatic fire fountains were likely the dominant mechanism for transfer of HCl to the stratosphere, and phreatomagmatic eruptions would not have dramatically affected the stratospheric ozone cycle (Beerling et al., 2007; Black et al., 2012, 2014b).

Sulfur dioxide is soluble as well, but it is less soluble than HCl (Tabazadeh and Turco, 1993; Textor et al., 2003). Sulfur degassing can be less efficient during phreatomagmatic than magmatic fragmentation (Ross et al., 2008). However, in contrast to HCl, only a negligible proportion of the SO_2 that reaches the plume dissolves in water or ice particles (Tabazadeh and Turco, 1993; Textor et al., 2003). Thus, if phreatomagmatic eruption columns did penetrate the tropopause, a large fraction of the sulfur emissions would likely reach the stratosphere (Textor et al., 2003). The resulting stratospheric aerosols would have resulted in a temporarily increased optical depth and cooler temperatures in the Northern Hemisphere (e.g., Stothers et al., 1986; Oman et al., 2005; Black et al., 2014b). Recently, Callegaro et al. (2014) revisited the possibility that high sulfur emissions could be an important link between large igneous province eruptions and mass extinction events.

The pipe eruptions described by Svensen et al. (2009) are an unusual feature of the Siberian Traps large igneous province. They may have released large quantities of CH_3Cl, CH_4, and other metamorphic gases, many of which could yield global chemical effects even if emitted to the troposphere (Black et al., 2014b). However, as discussed herein, the pipe eruptions have not yet been conclusively related to the more broadly distributed volcaniclastic rocks that are the focus of this paper. The potential environmental effects of the pipe eruptions are discussed at greater length in Svensen et al. (2004), Svensen et al. (2009), and Black et al. (2014b).

Finally, we speculate regarding the weathering of the volcaniclastic rocks. The volcaniclastic rocks are more porous, less well consolidated, and more susceptible to physical and chemical weathering than the lava flows (Büchl and Gier, 2003). Their total volume is also very large (Ross et al., 2005). Because CO_2 is relatively inert in the atmosphere, the eruptive style and altitude of injection do not determine the environmental effects of volcanic CO_2 emissions (e.g., Wignall, 2001). However, if the volcaniclastic rocks promoted rapid weathering, they may have expedited drawdown of atmospheric CO_2 (Dessert et al., 2001, 2003; Black et al., 2015). Furthermore, Meyer et al. (2011) have argued that high productivity in the surface ocean delayed benthic recovery from the end-Permian mass extinction. Relatively rapid weathering of the volcaniclastic rocks may have provided a larger-than-normal flux of nutrients to Permian–Triassic oceans, fueling this surface productivity. Rothman et al. (2014) have suggested that Ni from the Siberian Traps fueled a surge in methanogenesis. In these scenarios, the weathering of the volcaniclastic rocks may have been as environmentally significant as their emplacement.

CONCLUSIONS

Eruptions of large igneous provinces are rare but geologically significant events, with potentially cataclysmic environmental consequences. Here, we have focused on the Siberian Traps, which is one of the most voluminous continental flood basalt provinces to erupt in the Phanerozoic (e.g., Malich et al., 1974; Reichow et al., 2009). Siberian Traps magmatism has been linked to the end-Permian mass extinction (e.g., Campbell et al., 1992), the most severe loss of floral and faunal diversity in Earth's history (Erwin, 1993).

The origins of Siberian Traps volcaniclastic rocks carry implications for the release of volcanic gases, and the fate of those volatile species governs the environmental impacts of magmatism. Recent research has shown that magmatic fire fountaining likely delivers sporadic injections of gas to the stratosphere during high-latitude large igneous province eruptions like the Siberian Traps (Glaze et al., 2015). In this work, we use volcanological and paleomagnetic data to investigate the origin of Siberian Traps volcaniclastic rocks. While many of the volcaniclastic rocks are most consistent with nonexplosive to weakly explosive lava-water interactions, we argue that a significant fraction of the Siberian Traps volcaniclastic rocks originated from phreatomagmatic eruptions. Whereas HCl is preferentially removed from water-rich eruptive plumes, the majority of SO_2 does not partition into water or ice particles (Tabazadeh and Turco, 1993; Textor et al., 2003). Thus, if eruption columns above these phreatomagmatic vents reached the tropopause, they would have supplemented gases delivered by fire fountaining with an additional flux of sulfur to the stratosphere.

ACKNOWLEDGMENTS

This study was funded by National Science Foundation Continental Dynamics (grant number EAR-0807585), by the Russian Foundation for Basic Research (grant numbers 13-05-12030, 15-35-20599, and 14-05-31447) and the Ministry of Education and Science of the Russian Federation (grant number 14.Z50.31.0017), and by the Massachusetts Institute of Technology Wade Fund. The authors benefited from careful, thoughtful reviews by Pierre-Simon Ross and two anonymous reviewers, and from the skilled editorial supervision of A. Hope Jahren and Benjamin Laabs. Vladimir Pavlov, Anna Fetisova, Sam Bowring, and Seth Burgess were valued collaborators during field work, and Seth Burgess collected sample S10-2.5 from the Severnaya River. Bernhard Peucker-Ehrenbrink provided generous assistance with the electric pulse disaggregator at Woods Hole Oceanographic Institution. Sonia Tikoo, Roger Fu, and Kyle Bradley shared expert perspectives on the paleomagnetic analyses, and Steve Self offered valuable comments on the volcanology. Mehmet Onbasli assisted with vibrating sample magnetometer measurements in the Ross laboratory at Massachusetts Institute of Technology. The authors also gratefully thank Brenda Carbone for administrative help.

REFERENCES CITED

Aramaki, S., and Akimoto, S., 1957, Temperature estimation of pyroclastic deposits by natural remanent magnetism: American Journal of Science, v. 255, no. 9, p. 619–627, doi:10.2475/ajs.255.9.619.

Batiza, R., and White, J.D., 2000, Submarine lavas and hyaloclastite, *in* Sigurdsson, H., ed., Encyclopedia of Volcanoes: San Diego, California, Academic Press, p. 361–381.

Beerling, D.J., Harfoot, M., Lomax, B., and Pyle, J.A., 2007, The stability of the stratospheric ozone layer during the end-Permian eruption of the Siberian Traps: Philosophical Transactions of the Royal Society A–Mathematical Physical and Engineering Sciences, v. 365, no. 1856, p. 1843–1866.

Bergh, S.G., and Sigvaldason, G.E., 1991, Pleistocene mass-flow deposits of basaltic hyaloclastite on a shallow submarine shelf, South Iceland: Bulletin of Volcanology, v. 53, no. 8, p. 597–611, doi:10.1007/BF00493688.

Black, B.A., Elkins-Tanton, L.T., Rowe, M.C., and Peate, I.U., 2012, Magnitude and consequences of volatile release from the Siberian Traps: Earth and Planetary Science Letters, v. 317–318, p. 363–373, doi:10.1016/j.epsl.2011.12.001.

Black, B.A., Hauri, E.H., Elkins-Tanton, L.T., and Brown, S.M., 2014a, Sulfur isotopic evidence for sources of volatiles in Siberian Traps magmas: Earth and Planetary Science Letters, v. 394, p. 58–69, doi:10.1016/j.epsl.2014.02.057.

Black, B.A., Lamarque, J.F., Shields, C.A., Elkins-Tanton, L.T., and Kiehl, J.T., 2014b, Acid rain and ozone depletion from pulsed Siberian Traps magmatism: Geology, v. 42, p. 67–70.

Black, B.A., Lamarque, J., Shields, C.A., Elkins-Tanton, L.T., and Kiehl, J.T., 2015, Environmental effects of large igneous province magmatism: A Siberian perspective, *in* Schmidt, A., Fristad, K.E., and Elkins-Tanton, L.T., eds., Volcanism and Global Environmental Change: Cambridge, UK, Cambridge University Press, p. 307–320.

Brown, R.J., Blake, S., Thordarson, T., and Self, S., 2014, Pyroclastic edifices record vigorous lava fountains during the emplacement of a flood basalt flow field, Roza Member, Columbia River Basalt Province, USA: Geological Society of America Bulletin, v. 126, p. 875–891.

Büchl, A., and Gier, S., 2003, Petrogenesis and alteration of tuffs associated with continental flood basalts from Putorana, northern Siberia: Geological Magazine, v. 140, no. 6, p. 649–659, doi:10.1017/S0016756803008392.

Burgess, S.D., 2014, High-Precision U/Pb Geochronology of Large Igneous Provinces and Mass Extinctions: Testing Coincidence and Causation: Cambridge, Massachusetts, Massachusetts Institute of Technology, 250 p.

Burgess, S.D., Bowring, S., and Shen, S., 2014, High-precision timeline for Earth's most severe extinction: Proceedings of the National Academy of Sciences of the United States of America, v. 111, no. 9, p. 3316, doi:10.1073/pnas.1317692111.

Büttner, R., Dellino, P., and Zimanowski, B., 1999, Identifying magma–water interaction from the surface features of ash particles: Nature, v. 401, no. 6754, p. 688–690, doi:10.1038/44364.

Callegaro, S., Baker, D.R., De Min, A., Marzoli, A., Geraki, K., Bertrand, H., Viti, C., and Nestola, F., 2014, Micro-analyses link sulfur from large igneous provinces and Mesozoic mass extinctions: Geology, doi:10.1130/G35983.1 (in press).

Campbell, I.H., Czamanske, G.K., Fedorenko, V.A., Hill, R.I., and Stepanov, V., 1992, Synchronism of the Siberian Traps and the Permian-Triassic boundary: Science, v. 258, no. 5089, p. 1760–1763, doi:10.1126/science.258.5089.1760.

Cioni, R., Gurioli, L., Lanza, R., and Zanella, E., 2004, Temperatures of the AD 79 pyroclastic density current deposits (Vesuvius, Italy): Journal of Geophysical Research–Solid Earth (1978–2012), v. 109, no. B2, B02207, doi:10.1029/2002JB002251.

Czamanske, G.K., Gurevitch, A., Fedorenko, V., and Simonov, O., 1998, Demise of the Siberian plume: Paleogeographic and paleotectonic reconstruction from the prevolcanic and volcanic record, north-central Siberia: International Geology Review, v. 40, no. 2, p. 95–115, doi:10.1080/00206819809465200.

Dessert, C., Dupré, B., François, L.M., Schott, J., Gaillardet, J., Chakrapani, G., and Bajpai, S., 2001, Erosion of Deccan Traps determined by river geochemistry: Impact on the global climate and the $^{87}Sr/^{86}Sr$ ratio of seawater: Earth and Planetary Science Letters, v. 188, no. 3, p. 459–474, doi:10.1016/S0012-821X(01)00317-X.

Dessert, C., Dupré, B., Gaillardet, J., François, L.M., and Allegre, C.J., 2003, Basalt weathering laws and the impact of basalt weathering on the global carbon cycle: Chemical Geology, v. 202, no. 3, p. 257–273, doi:10.1016/j.chemgeo.2002.10.001.

Dunlop, D.J., 1990, Developments in rock magnetism: Reports on Progress in Physics, v. 53, no. 6, p. 707.

Dunlop, D.J., and Özdemir, Ö., 2001, Rock Magnetism: Fundamentals and Frontiers: Cambridge, UK, Cambridge University Press, Studies in Magnetism 3, 596 p.

Erwin, D.H., 1993, The Great Paleozoic Crisis: Life and Death in the Permian: New York, Columbia University Press, 327 p.

Fedorenko, V., 1994, Evolution of magmatism as reflected in the volcanic sequence of the Noril'sk region, *in* Lightfoot, P.C., and Naldrett, A.J., eds., Proceedings of the Sudbury-Noril'sk Symposium: Ontario Geological Survey Special Publication 5, p. 171–184.

Fedorenko, V.A., and Czamanske, G.K., 1997, Results of new field and geochemical studies of the volcanic and intrusive rocks of the Maymecha-Kotuy area, Siberian flood-basalt province, Russia: International Geology Review, v. 39, p. 479–531, doi:10.1080/00206819709465286.

Fedorenko, V.A., Lightfoot, P.C., Naldrett, A.J., Czamanske, G.K., Hawkesworth, C.J., Wooden, J.L., and Ebel, D.S., 1996, Petrogenesis of the flood-basalt sequence at Noril'sk, north central Siberia: International Geology Review, v. 38, no. 2, p. 99–135, doi:10.1080/00206819709465327.

Fedorenko, V., Czamanske, G., Zen'ko, T., Budahn, J., and Siems, D., 2000, Field and geochemical studies of the melilite-rearing Arydzhangsky Suite, and an overall perspective on the Siberian alkaline-ultramafic flood-volcanic rocks: International Geology Review, v. 42, no. 9, p. 769–804, doi:10.1080/00206810009465111.

Glaze, L., Self, S., Schmidt, A., and Hunter, S., 2015, Assessing eruption column height in ancient flood basalt eruptions: Earth and Planetary Science Letters (in press).

Grise, K.M., Thompson, D.W., and Birner, T., 2010, A global survey of static stability in the stratosphere and upper troposphere: Journal of Climate, v. 23, no. 9, p. 2275–2292, doi:10.1175/2009JCLI3369.1.

Gurevitch, E.L., Heunemann, C., Rad'ko, V., Westphal, M., Bachtadse, V., Pozzi, J.P., and Feinberg, H., 2004, Palaeomagnetism and magnetostratigraphy of the Permian–Triassic northwest central Siberian Trap Basalts: Tectonophysics, v. 379, no. 1–4, p. 211–226, doi:10.1016/j.tecto.2003.11.005.

Heiken, G., 1972, Morphology and petrography of volcanic ashes: Geological Society of America Bulletin, v. 83, no. 7, p. 1961, doi:10.1130/0016-7606(1972)83[1961:MAPOVA]2.0.CO;2.

Held, I.M., 1982, On the height of the tropopause and the static stability of the troposphere: Journal of the Atmospheric Sciences, v. 39, no. 2, p. 412–417, doi:10.1175/1520-0469(1982)039<0412:OTHOTT>2.0.CO;2.

Heunemann, C., 2003, Direction and Intensity of Earth's Magnetic Field at the Permo-Triassic Boundary [Ph.D. thesis]: Münich, Ludwig-Maximilians Universität, 116 p.

Heunemann, C., Krása, D., Soffel, H.C., Gurevitch, E., and Bachtadse, V., 2004, Directions and intensities of the Earth's magnetic field during a reversal: Results from the Permo-Triassic Siberian Trap basalts, Russia: Earth and Planetary Science Letters, v. 218, no. 1, p. 197–213, doi:10.1016/S0012-821X(03)00642-3.

Hoblitt, R.P., and Kellogg, K.S., 1979, Emplacement temperatures of unsorted and unstratified deposits of volcanic rock debris as determined by paleomagnetic techniques: Geological Society of America Bulletin, v. 90, no. 7, p. 633–642, doi:10.1130/0016-7606(1979)90<633:ETOUAU>2.0.CO;2.

Jerram, D.A., Single, R.T., Hobbs, R.W., and Nelson, C.E., 2009, Understanding the offshore flood basalt sequence using onshore volcanic facies analogues: An example from the Faroe–Shetland basin: Geological Magazine, v. 146, no. 3, p. 353–367, doi:10.1017/S0016756809005974.

Joachimski, M.M., Lai, X., Shen, S., Jiang, H., Luo, G., Chen, B., Chen, J., and Sun, Y., 2012, Climate warming in the latest Permian and the Permian–Triassic mass extinction: Geology, v. 40, no. 3, p. 195–198, doi:10.1130/G32707.1.

Kamo, S.L., Czamanske, G.K., Amelin, Y., Fedorenko, V.A., Davis, D.W., and Trofimov, V.R., 2003, Rapid eruption of Siberian flood-volcanic rocks and evidence for coincidence with the Permian-Triassic boundary and mass extinction at 251 Ma: Earth and Planetary Science Letters, v. 214, no. 1–2, p. 75–91, doi:10.1016/S0012-821X(03)00347-9.

Kazansky, A.Yu, Metelkin, D.V., Yu Bragin, V., and Kungurtsev, L.V., 2005, Paleomagnetism of the Permian-Triassic traps from the Kuznetsk Basin, southern Siberia: Russian Geology and Geophysics, v. 46, no. 11, p. 1089–1102.

Kent, D.V., Ninkovich, D., Pescatore, T., and Sparks, S.R., 1981, Palaeomagnetic determination of emplacement temperature of Vesuvius AD 79 pyroclastic deposits: Nature, v. 290, no. 5805, p. 393–396, doi:10.1038/290393a0.

Kirschvink, J., 1980, The least-squares line and plane and the analysis of palaeomagnetic data: Geophysical Journal International, v. 62, no. 3, p. 699–718, doi:10.1111/j.1365-246X.1980.tb02601.x.

Koyaguchi, T., and Woods, A.W., 1996, On the formation of eruption columns following explosive mixing of magma and surface-water: Journal of Geophysical Research–Solid Earth, v. 101, no. B3, p. 5561–5574, doi:10.1029/95JB01687.

Latyshev, A.V., Veselovskiy, R.V., Ivanov, A.V., Fetisova, A.M., and Pavlov, V.E., 2013, Short intense bursts in magmatic activity in the south of Siberian Platform (Angara-Taseeva Depression): The paleomagnetic evidence: Izvestiya: Physics of the Solid Earth, v. 49, no. 6, p. 823–835, doi:10.1134/S1069351313050030.

Levitan, M.M., and Zastoina, A.N., 1985, Federal Geological Map USSR: Tunguska Series, Q-47 Xxxv, Xxxvi.

Lind, E.N., Kropotov, S.V., Czamanske, G.K., Gromme, S.C., and Fedorenko, V.A., 1994, Paleomagnetism of the Siberian flood basalts of the Noril'sk area: A constraint on eruption duration: International Geology Review, v. 36, no. 12, p. 1139–1150.

Malich, N.S., Tazihin, N.N., Tuganova, E.V., Bunzen, E.A., Kulikova, N.G., and Safonova, I.V.A., 1974, Map of Geological Formations of the Siberian Platform Cover: scale 1:1,500,000.

McClelland, E., and Druitt, T.H., 1989, Palaeomagnetic estimates of emplacement temperatures of pyroclastic deposits on Santorini, Greece: Bulletin of Volcanology, v. 51, no. 1, p. 16–27, doi:10.1007/BF01086758.

McClelland, E., Wilson, C.J.N., and Bardot, L., 2004, Palaeotemperature determinations for the 1.8-ka Taupo ignimbrite, New Zealand, and implications for the emplacement history of a high-velocity pyroclastic flow: Bulletin of Volcanology, v. 66, no. 6, p. 492–513, doi:10.1007/s00445-003-0335-5.

McClintock, M., and White, J.D., 2006, Large phreatomagmatic vent complex at Coombs Hills, Antarctica: Wet, explosive initiation of flood basalt volcanism in the Ferrar-Karoo LIP: Bulletin of Volcanology, v. 68, no. 3, p. 215–239, doi:10.1007/s00445-005-0001-1.

Meyer, K., Yu, M., Jost, A., Kelley, B., and Payne, J., 2011, $\delta^{13}C$ evidence that high primary productivity delayed recovery from end-Permian mass extinction: Earth and Planetary Science Letters, v. 302, no. 3, p. 378–384, doi:10.1016/j.epsl.2010.12.033.

Naumov, V.A., and Ankudimova, L.A., 1995, Palynological complexes and age of volcanic sediments of the Angara-Katanga District, middle Angara region: Geology and Geophysics, v. 36, no. 1.

Oman, L., Robock, A., Stenchikov, G., Schmidt, G.A., and Ruedy, R., 2005, Climatic response to high-latitude volcanic eruptions: Journal of Geophysical Research–Atmospheres (1984–2012), v. 110, no. D13.

Paterson, G.A., Roberts, A.P., Mac Niocaill, C., Muxworthy, A.R., Gurioli, L., Viramonté, J.G., Navarro, C., and Weider, S., 2010, Paleomagnetic determination of emplacement temperatures of pyroclastic deposits: An under-utilized tool: Bulletin of Volcanology, v. 72, no. 3, p. 309–330, doi:10.1007/s00445-009-0324-4.

Pavlov, V., Bazhenov, M., and Veselovsky, R., 2007, Paleomagnetism of the Siberian Traps: New data and a

new overall 250 Ma pole for Siberia: Tectonophysics, v. 443, no. 1, p. 72–92.

Pavlov, V., Fluteau, F., Veselovskiy, R., Fetisova, A., and Latyshev, A., 2011, Secular geomagnetic variations and volcanic pulses in the Permian-Triassic traps of the Norilsk and Maimecha-Kotui Provinces: Izvestiya: Physics of the Solid Earth, v. 47, no. 5, p. 402–417, doi:10.1134/S1069351311040070.

Peate, I.U., and Bryan, S.E., 2008, Re-evaluating plume-induced uplift in the Emeishan large igneous province: Nature Geoscience, v. 1, no. 9, p. 625–629, doi:10.1038/ngeo281.

Pierson, T.C., Daag, A.S., Delos Reyes, P., Regalado, M.T.M., Solidum, R.U., and Tubianosa, B.S., 1996, Flow and deposition of posteruption hot lahars on the east side of Mount Pinatubo, July–October 1991, *in* Newhall, C.G., and Punongbayan, R.S., eds., Fire and Mud: Eruptions and Lahars of Mount Pinatubo, Philippines: Florham Park, New Jersey, Washington Press, p. 921–950.

Pinto, J.P., Turco, R.P., and Toon, O.B., 1989, Self-limiting physical and chemical effects in volcanic-eruption clouds: Journal of Geophysical Research, ser. D, Atmospheres, v. 94, no. D8, p. 11,165–11,174, doi:10.1029/JD094iD08p11165.

Porreca, M., Mattei, M., MacNiocaill, C., Giordano, G., McClelland, E., and Funiciello, R., 2008, Paleomagnetic evidence for low-temperature emplacement of the phreatomagmatic Peperino Albano ignimbrite (Colli Albani volcano, central Italy): Bulletin of Volcanology, v. 70, no. 7, p. 877–893, doi:10.1007/s00445-007-0176-8.

Pullaiah, G., Irving, E., Buchan, K., and Dunlop, D., 1975, Magnetization changes caused by burial and uplift: Earth and Planetary Science Letters, v. 28, no. 2, p. 133–143, doi:10.1016/0012-821X(75)90221-6.

Reichow, M.K., Pringle, M.S., Al'Mukhamedov, A.I., Allen, M.B., Andreichev, V.L., Buslov, M.M., and Davies, C.E., 2009, The timing and extent of the eruption of the Siberian Traps large igneous province: Implications for the end-Permian environmental crisis: Earth and Planetary Science Letters, v. 277, no. 1–2, p. 9–20, doi:10.1016/j.epsl.2008.09.030.

Ross, P., and White, J.D., 2005, Mafic, large-volume, pyroclastic density current deposits from phreatomagmatic eruptions in the Ferrar large igneous province, Antarctica: The Journal of Geology, v. 113, no. 6, p. 627–649, doi:10.1086/449324.

Ross, P., and White, J.D., 2006, Debris jets in continental phreatomagmatic volcanoes: A field study of their subterranean deposits in the Coombs Hills vent complex, Antarctica: Journal of Volcanology and Geothermal Research, v. 149, no. 1, p. 62–84, doi:10.1016/j.jvolgeores.2005.06.007.

Ross, P., Peate, I.U., McClintock, M.K., Xu, Y.G., Skilling, I.P., White, J.D.L., and Houghton, B.F., 2005, Mafic volcaniclastic deposits in flood basalt provinces: A review: Journal of Volcanology and Geothermal Research, v. 145, no. 3–4, p. 281–314, doi:10.1016/j.jvolgeores.2005.02.003.

Ross, P., White, J.D., and McClintock, M., 2008, Geological evolution of the Coombs–Allan Hills area, Ferrar large igneous province, Antarctica: Debris avalanches, mafic pyroclastic density currents, phreatocauldrons: Journal of Volcanology and Geothermal Research, v. 172, no. 1, p. 38–60, doi:10.1016/j.jvolgeores.2005.11.011.

Rothman, D.H., Fournier, G.P., French, K.L., Alm, E.J., Boyle, E.A., Cao, C., and Summons, R.E., 2014, Methanogenic burst in the end-Permian carbon cycle: Proceedings of the National Academy of Sciences, v. 111, no. 15, p. 5462–5467.

Rudakova, A., and Krivolutskaya, N., 2009, Structural and textural specific features of rocks of Trap Rock Association in the Norilsk Trough (NW of Siberian platform): Moscow University Geology Bulletin, v. 64, no. 6, p. 364–375, doi:10.3103/S0145875209060052.

Schult, A., 1970, Effect of pressure on the Curie temperature of titanomagnetites [(1− x)· Fe 3 O 4− x· TiFe 2 O 4]: Earth and Planetary Science Letters, v. 10, no. 1, p. 81–86.

Schumacher, R., and Schmincke, H.U., 1995, Models for the origin of accretionary lapilli: Bulletin of Volcanology, v. 56, no. 8, p. 626–639, doi:10.1007/BF00301467.

Self, S., Thordarson, T., and Keszthelyi, L., 1997, Emplacement of continental flood basalt lava flows, *in* Mahoney, J.J., and Coffin, M.F., eds., Large Igneous Provinces: Continental, Oceanic, and Planetary Flood Volcanism: American Geophysical Union Geophysical Monograph 100, p. 381–410.

Sharma, M., 1997, Siberian Traps, *in* Mahoney, J.J., and Coffin, M.F., eds., Large Igneous Provinces: Continental, Oceanic, and Planetary Flood Volcanism: American Geophysical Union Geophysical Monograph 100, p. 273–296.

Sheridan, M.F., and Wang, Y., 2005, Cooling and welding history of the Bishop Tuff in Adobe Valley and Chidago canyon, California: Journal of Volcanology and Geothermal Research, v. 142, no. 1, p. 119–144.

Stothers, R.B., Wolff, J.A., Self, S., and Rampino, M.R., 1986, Basaltic fissure eruptions, plume heights, and atmospheric aerosols: Geophysical Research Letters, v. 13, no. 8, p. 725–728, doi:10.1029/GL013i008p00725.

Sun, Y., Joachimski, M.M., Wignall, P.B., Yan, C., Chen, Y., Jiang, H., Wang, L., and Lai, X., 2012, Lethally hot temperatures during the Early Triassic greenhouse: Science (New York, N.Y.), v. 338, no. 6105, p. 366–370, doi:10.1126/science.1224126.

Svensen, H., Planke, S., Malthe-Sørenssen, A., Jamtveit, B., Myklebust, R., Eidem, T.R., and Rey, S.S., 2004, Release of methane from a volcanic basin as a mechanism for initial Eocene global warming: Nature, v. 429, no. 6991, p. 542–545, doi:10.1038/nature02566.

Svensen, H., Planke, S., Polozov, A.G., Schmidbauer, N., Corfu, F., Podladchikov, Y.Y., and Jamtveit, B., 2009, Siberian gas venting and the end-Permian environmental crisis: Earth and Planetary Science Letters, v. 277, no. 3–4, p. 490–500, doi:10.1016/j.epsl.2008.11.015.

Tabazadeh, A., and Turco, R.P., 1993, Stratospheric chlorine injection by volcanic-eruptions—HCl scavenging and implications for ozone: Science, v. 260, no. 5111, p. 1082–1086, doi:10.1126/science.260.5111.1082.

Textor, C., Graf, H.F., Herzog, M., and Oberhuber, J.M., 2003, Injection of gases into the stratosphere by explosive volcanic eruptions: Journal of Geophysical Research, ser. D, Atmospheres, v. 108, no. D19, 4606, doi:10.1029/2002JD002987.

Thordarson, T., and Self, S., 1993, The Laki (Skaftár Fires) and Grímsvötn eruptions in 1783–1785: Bulletin of Volcanology, v. 55, no. 4, p. 233–263, doi:10.1007/BF00624353.

Thordarson, T., and Self, S., 1998, The Roza Member, Columbia River Basalt Group: A gigantic pahoehoe lava flow field formed by endogenous processes?: Journal of Geophysical Research, v. 103, no. B11, p. 27,411–27,445.

Thordarson, T., Larsen, G., Steinthorsson, S., and Self, S., 2003, The 1783–1785 AD Laki-Grímsvötn eruptions II: Appraisal based on contemporary accounts: Jökull, v. 53, p. 11–47.

Veselovsky, R., Gallet, Y., and Pavlov, V., 2003, Paleomagnetism of traps in the Podkamennaya Tunguska and Kotui River Valleys: Implications for the post-Paleozoic relative movements of the Siberian and East European platforms: Izvestiya: Physics of the Solid Earth, v. 39, no. 10, p. 856–871.

Veselovskiy, R.V., Konstantinov, K.M., Latyshev, A.V., and Fetisova, A.M., 2012, Paleomagnetism of the trap intrusive bodies in arctic Siberia: Geological and methodical implications: Izvestiya: Physics of the Solid Earth, v. 48, no. 9–10, p. 738–750, doi:10.1134/S1069351312090054.

Watson, G.S., 1956, A test for randomness of directions: Geophysical Supplements to the Monthly Notices of the Royal Astronomical Society, v. 7, no. 4, p. 160–161.

White, J.D.L., and Houghton, B.F., 2006, Primary volcaniclastic rocks: Geology, v. 34, no. 8, p. 677–680, doi:10.1130/G22346.1.

White, J.D.L., and McClintock, M.K., 2001, Immense vent complex marks flood-basalt eruption in a wet, failed rift: Coombs Hills, Antarctica: Geology, v. 29, no. 10, p. 935–938, doi:10.1130/0091-7613(2001)029<0935:IVCMFB>2.0.CO;2.

White, J., Bryan, S., Ross, P., Self, S., and Thordarson, T., 2009, Physical volcanology of continental large igneous provinces: Update and review, *in* Thordarson, T., Self, S., Larsen, G., Rowland, S.K., and Hoskuldsson, A., eds., Studies in Volcanology: The Legacy of George Walker: London, U.K., Geological Society of London, p. 291–321.

White, R.V., 2002, Earth's biggest 'whodunnit': Unravelling the clues in the case of the end-Permian mass extinction: Philosophical Transactions of the Royal Society of London, ser. A, Mathematical Physical and Engineering Sciences, v. 360, no. 1801, p. 2963–2985.

Wignall, P.B., 2001, Large igneous provinces and mass extinctions: Earth-Science Reviews, v. 53, no. 1–2, p. 1–33, doi:10.1016/S0012-8252(00)00037-4.

Wignall, P.B., Sun, Y., Bond, D.P., Izon, G., Newton, R.J., Védrine, S., and Widdowson, M., 2009, Volcanism, mass extinction, and carbon isotope fluctuations in the Middle Permian of China: Science, v. 324, no. 5931, p. 1179–1182, doi:10.1126/science.1171956.

Williams, S.N., Schaefer, S.J., Marta Lucia Calvache, V., and Lopez, D., 1992, Global carbon dioxide emission to the atmosphere by volcanoes: Geochimica et Cosmochimica Acta, v. 56, no. 4, p. 1765–1770, doi:10.1016/0016-7037(92)90243-C.

Wohletz, K.H., 1983, Mechanisms of hydrovolcanic pyroclast formation—Grain-size, scanning electron-microscopy, and experimental studies: Journal of Volcanology and Geothermal Research, v. 17, no. 1–4, p. 31–63, doi:10.1016/0377-0273(83)90061-6.

Wooden, J.L., Czamanske, G.K., Fedorenko, V.A., Arndt, N.T., Chauvel, C., Bouse, R.M., King, B.S.W., Knight, R.J., and Siems, D.F., 1993, Isotopic and trace-element constraints on mantle and crustal contributions to Siberian continental flood basalts, Norilsk area, Siberia: Geochimica et Cosmochimica Acta, v. 57, no. 15, p. 3677–3704, doi:10.1016/0016-7037(93)90149-Q.

Yamagishi, H., 1991, Morphological and sedimentological characteristics of the Neogene submarine coherent lavas and hyaloclastites in southwest Hokkaido, Japan: Sedimentary Geology, v. 74, no. 1, p. 5–23, doi:10.1016/0037-0738(91)90032-9.

Zharkov, M.A., 1984, Paleozoic Salt Bearing Formations of the World: Springer Verlag.

Zolotukhin, V.V., and Almukhamedov, A.I., 1988, Traps of the Siberian Platform, *in* Macdougall, J.D., ed., Continental Flood Basalts: Dordrecht, Kluwer Academic Publishers, p. 273–310.

Science Editor: A. Hope Jahren
Associate Editor: Benjamin J.C. Laabs

Manuscript Received 7 April 2014
Revised Manuscript Received 10 January 2015
Manuscript Accepted 17 March 2015

Printed in the USA

Supplementary Materials

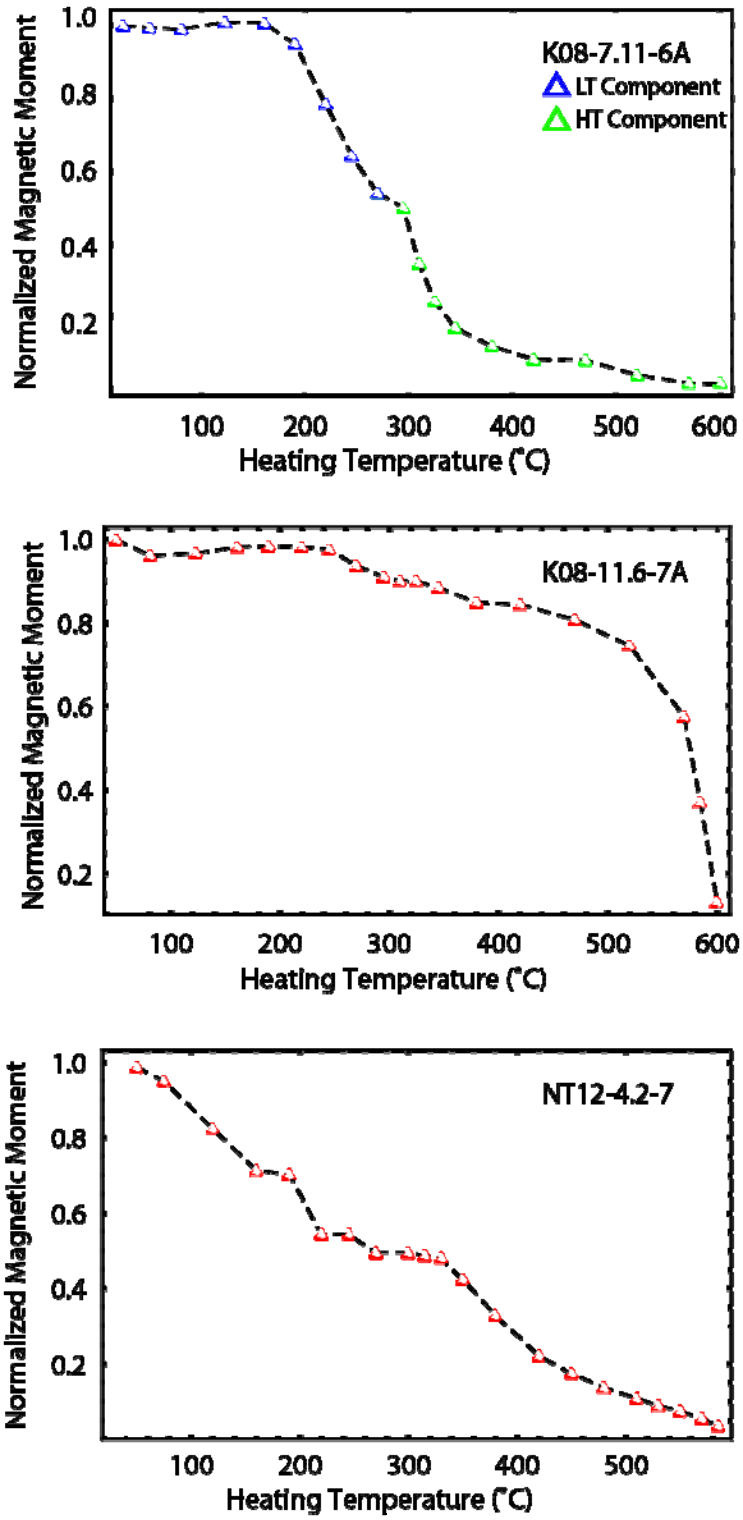

Supplementary Figure A1. Intensity of natural remanent magnetization during thermal

demagnetization for three clasts sampled from parent blocks K08-7.11, K08-11.6, and NT12-4.2.

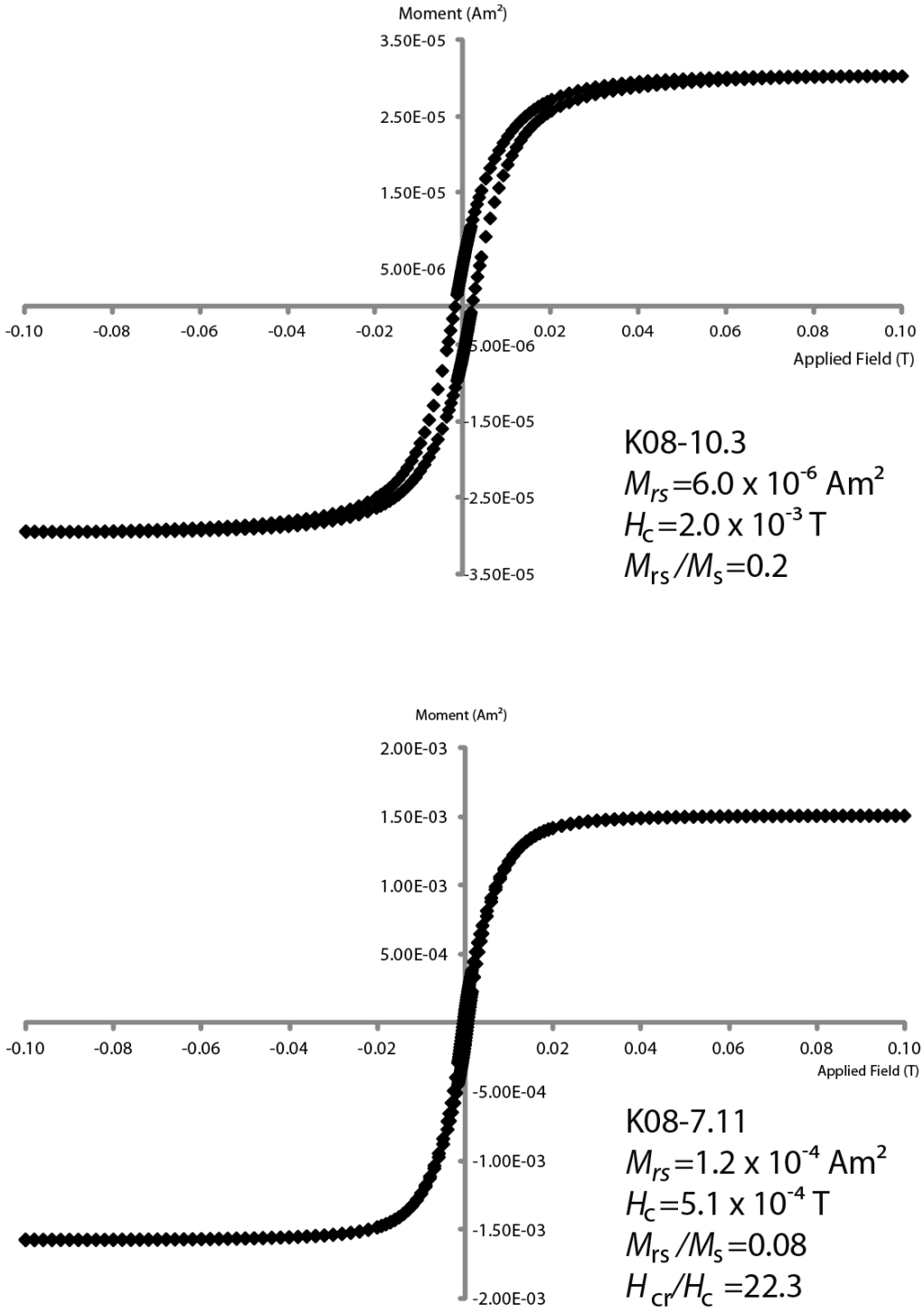

Supplementary Figure A2. Hysteresis loops for selected samples measured with a vibrating sample magnetometer, after correction for paramagnetic high field slope. H_{cr} and H_c were measured on different clasts from block K08-7.11.

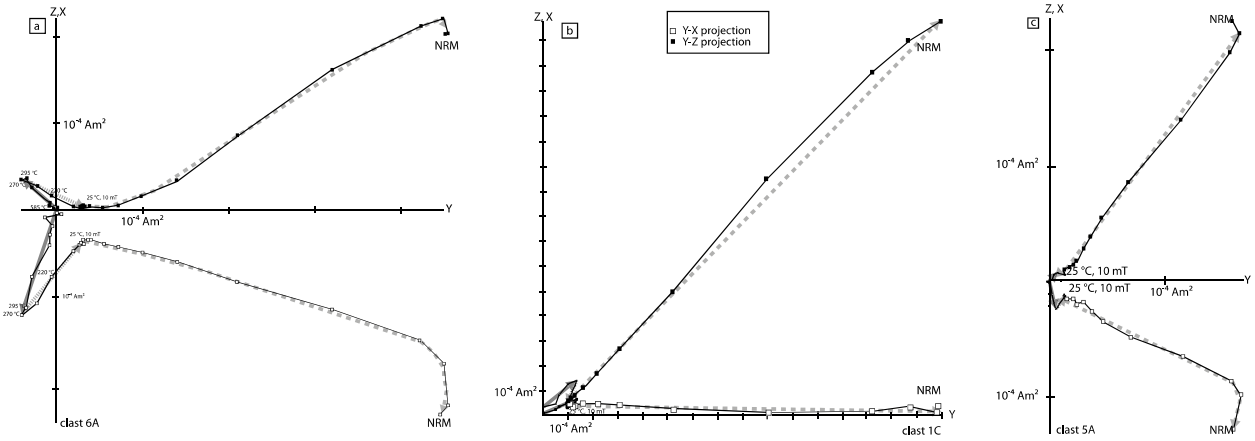

Supplementary Figure A3. AF demagnetization and NRM for clasts from parent block K08-7.11 shown in Figure 5 of the main text.

Sample	Clast	Component	Temperature Range (˚C)	Declination, Inclination (˚) *	*N* steps	MAD (˚)
K08-7.11	1A	LT	25 ˚C – 270 ˚C	213.1, 14.1	9	11.4
		HT	270 ˚C – 570 ˚C	52.7, -21.7	5	6.8
	1B	LT	25 ˚C – 270 ˚C	202.3, 14.1	9	6.4
		HT	270 ˚C – 585 ˚C	31.5, -21.9	6	4.8
	1C	LT	25 ˚C – 270 ˚C	201.6, 11.0	9	11.7
		HT	270 ˚C – 345 ˚C	44.5, -17.9	5	7.4
	2	LT	25 ˚C – 245 ˚C	174.5, -65.0	8	14.2
		HT	245 ˚C – 585 ˚C	42.7, 17.3	8	3.9
	3	LT	25 ˚C – 270 ˚C	60.2, 14.9	9	6.2
		HT	270 ˚C – 380 ˚C	247.1, -14.1	5	10.3
	5	LT	25 ˚C – 270 ˚C	31.3, 2.0	9	11.2
		HT	270 ˚C – 585 ˚C	164.7, -16.2	7	8.9
	6	LT	25 ˚C – 270 ˚C	39.7, 15.6	10	4.2
		HT	270 ˚C – 585 ˚C	198.4, -16.4	11	5.8
	7	LT	25 ˚C – 220 ˚C	346.4, -72.2	6	29.6
		HT	220 ˚C – 585 ˚C	100.5, 41.9	4	8.6
	8	HT	25 ˚C – 585 ˚C	70.4, -19.7	10	4.3
	9B	HT	25 ˚C – 585 ˚C	116.2, 31.6	19	1.5
	10A	LT	25 ˚C – 295 ˚C	79.6, 50.2	9	30.2
		HT	295 ˚C – 420 ˚C	109.7, -60.7	7	22.1
	11A	HT	25 ˚C – 350 ˚C	222.6, -28.9	12	3.4
K08-11.6	1A	HT	81 ˚C – 585 ˚C	198.4, 0.7	19	5.8
	1B	HT	50 ˚C – 585 ˚C	199.9, 1.7	19	4.9
	2	HT	25 ˚C – 600 ˚C	190.3, -3.0	14	5.2
	3A	HT	25 ˚C – 570 ˚C	193.9, 11.6	16	11.1
		VHT	570 ˚C – 620 ˚C	10.1, 21.3	5	12.3
	3B	HT	123 ˚C – 585 ˚C	205.8, 9.4	15	8.2
		VHT	585 ˚C – 620 ˚C	10.7, 16.9	4	6.6
	4A	HT	50 ˚C – 585 ˚C	194.9, 3.7	18	6.2
	4B	HT	50 ˚C – 600 ˚C	199.8, 4.6	17	6.6
	5	HT	25 ˚C – 585 ˚C	195.1, -3.4	20	3.9
	6	HT	123 ˚C – 585 ˚C	190.4, 8.7	16	7.0
	7	HT	50 ˚C – 600 ˚C	197.9, -2.5	20	7.2
	8	HT	81 ˚C – 620 ˚C	196.2, -2.5	19	3.9
K08-10.3	1A	HT	50 ˚C – 585 ˚C	348.5, -53.7	22	23.2 †
	1B	HT	50 ˚C – 585 ˚C	288.3, 21.1	21	7.1 †
	3	HT	50 ˚C – 585 ˚C	218.3, 1.2	13	5.2 †
	5	LT	50 ˚C – 530 ˚C	231.9, -25.5	12	13.1

		HT	550 ˚C – 585 ˚C	16.5, -33.9	3	4.8 †
	6A	HT	75 ˚C – 585 ˚C	29.8, -48.0	20	5.0 †
	6B	HT	50 ˚C – 585 ˚C	25.5, -38.3	21	6.8 †
	7A	HT	50 ˚C – 585 ˚C	226.3, -21.7	21	6.3 †
	7B	HT	50 ˚C – 585 ˚C	259.2, -46.1	17	3.9 †
	8	LT	50 ˚C – 220 ˚C	356.2, 81.8	7	26.6
NT12-4.2	1A	HT	50 ˚C – 585 ˚C	15.7, 10.6	18	2.5 †
	1B	HT	50 ˚C – 585 ˚C	10.8, 8.8	17	3.0 †
	2A	HT	50 ˚C – 585 ˚C	4.3, 18.6	19	1.9 †
	2B	HT	50 ˚C – 585 ˚C	5.2, 19.8	17	2.2 †
	3	HT	50 ˚C – 585 ˚C	7.2, 12.7	21	2.2 †
	4	HT	50 ˚C – 585 ˚C	8.5, 10.6	21	2.7 †
	5	HT	50 ˚C – 585 ˚C	14.4, 4.5	21	4.3 †
	6	HT	50 ˚C – 585 ˚C	352.9, 22.4	20	3.2 †
	7	HT	50 ˚C – 585 ˚C	6.8, 13.9	21	2.1 †
	8A	HT	50 ˚C – 585 ˚C	7.3, 6.5	21	3.8 †
	8B	HT	75 ˚C – 585 ˚C	6.7, 9.9	20	2.3 †
	9	HT	50 ˚C – 585 ˚C	9.8, 9.6	21	2.8 †
A10-A9B §	127	VLT	20 ˚C – 290 ˚C	345.9, 75.8	4	0.5
		HT	400 ˚C – 580 ˚C	71.7, 87.0	6	2.1
	128	VLT	20 ˚C – 290 ˚C	340.0, 69.2	4	3.4
		HT	350 ˚C – 600 ˚C	36.1, 78.4	8	3.9
	129	VLT	20 ˚C – 210 ˚C	306.8, 69.7	3	6.3
		HT	400 ˚C – 600 ˚C	208.9, 78.4	7	1.7
	130	HT	400 ˚C – 640 ˚C	231.6, 81.1	9	1.3
	131	VLT	20 ˚C – 210 ˚C	336.7, 62.1	3	4.0
		HT	400 ˚C – 600 ˚C	34.7, 86.6	9	1.5
	132	HT	350 ˚C – 600 ˚C	146.1, 86.3	8	1.2
	133	HT	350 ˚C – 520 ˚C	93.3, 81.5	5	1.4
	134	VLT	20 ˚C – 210 ˚C	50.6, 80.9	3	12.2
		HT	350 ˚C – 580 ˚C	127.0, 83.8	7	1.1
	136	HT	350 ˚C – 520 ˚C	357.0, 83.2	5	1.5
	138	HT	350 ˚C – 640 ˚C	99.3, 56.4	10	1.0
	139	HT	290 ˚C – 640 ˚C	49.4, 83.0	11	0.8
	140	VLT	20 ˚C – 210 ˚C	56.0, 81.4	3	13.3
		HT	400 ˚C – 620 ˚C	67.6, 77.4	8	1.2
	141	HT	400 ˚C – 640 ˚C	49.6, 75.9	9	1.9

** Note that orientations are relative except for sample A10-A9B; all other samples are unoriented relative to true geographic coordinates.*

† Indicates that the fit for this component was forced through the origin.

§ This sample was analyzed at Moscow State University with a JR-6 spinner magnetometer.

*Supplementary Table A1***.** Paleomagnetic components and fits. Note that S10-2-5 is not included in the table above because clasts did not yield coherent components of magnetization.

Sample	**Component**	***N***	**Watson R**	**Watson $R_{95\%}$**	**Conglomerate Test**
A10-A9B	VLT	*6*	5.88	3.85	Fail
	HT	*13*	12.75	5.82	Fail
K08-7.11	LT	*8*	6.65	4.48	Fail
	HT	*10*	3.76	5.03	Pass
K08-10.3	HT	*6*	2.45	3.85	Pass
K08-11.6	HT	*8*	7.85	4.48	Fail
NT12-4.2	HT	*9*	8.92	5.59	Fail

Supplementary Table A2. Results of Watson's (1956) test. If *R* exceeds the 95% significance value $R_{95\%}$, the clasts are non-randomly magnetized and the sample fails the conglomerate test. We did not include matrix samples in the Watson test calculation.

Supplementary References

Watson, G., 1956, A Test for Randomness of Directions: Geophysical Supplements to the Monthly Notices of the Royal Astronomical Society, v. 7, p. 160-161.